Manuscript Click here to view linked References

Title:

Discrete cis-acting element regulates developmentally timed gene-lamina relocation and neural progenitor competence *in vivo*.

Authors list:

Tanguy Lucas[1]*, Terry L. Hafer [1,2,]*, Harrison Zhang [1], Natalia Molotkova [1], and Minoree Kohwi[3‡†]

Affiliations:

1. Columbia University, Department of Neuroscience, Mortimer B. Zuckerman Institute Mind Brain Behavior, New York, NY, 10027 United States

2. Current affiliation: Division of Basic Sciences, Fred Hutchinson Cancer Research Center, Seattle, WA 98109, United States; Molecular and Cellular Biology Program, University of Washington, Seattle, WA 98195, United States

3. Columbia University, Department of Neuroscience, Mortimer B. Zuckerman Institute Mind Brain Behavior, New York, NY, 10027 United States; Kavli Institute for Brain Science, Columbia University, New York, NY, 10027 United States.

*These authors contributed equally

‡ Lead contact

†Correspondence: mk3632@columbia.edu.

Summary:

The nuclear lamina is typically associated with transcriptional silencing, and peripheral relocation of genes highly correlates with repression. However, the DNA sequences and proteins regulating gene-lamina interactions are largely unknown. Exploiting the developmentally-timed *hunchback* gene movement to the lamina in *Drosophila* neuroblasts, we identified a 250bp intronic element (IE) both necessary and sufficient for relocation. The IE can target a reporter transgene to the lamina and silence it. Endogenously, however, *hunchback* is already repressed prior to relocation. Instead, IE-mediated relocation confers a heritably-silenced gene state refractory to activation in descendent neurons, which terminates neuroblast competence to specify early-born identity. Surprisingly, we found Polycomb group chromatin factors bind the IE and are required for lamina-relocation, revealing a nuclear architectural role distinct from

their well-known function in transcriptional repression. Together, our results uncover *in vivo* mechanisms underlying neuroblast competence and lamina-association in heritable gene silencing.

Introduction:

The metazoan genome is non-randomly distributed in nuclear space, and its three-dimensional organization is considered to play a critical role in gene regulation. High throughput studies have shown that higher order genome architectures exist across species and are likely important for animal development (Bonev et al., 2017; Lucas and Kohwi, 2019; Van Bortle and Corces, 2013). Though global changes in genome organization have been observed in the context of development, at the smallest scale of individual genes, little is known about how such reorganization translates to gene regulation. This is at least in part due to the fact that genome architecture is highly context specific and thus requires cell type and stage-specific analyses *in vivo*. However, lack of model systems that are amenable to both genetic dissection and genome architecture analyses in intact animals is a major challenge to address this important question in a biologically meaningful manner. To tackle this, we used neural progenitors (neuroblasts) of intact *Drosophila* embryos, in which we exploited their well characterized lineages to study mechanisms of gene regulation through genome architecture reorganization *in vivo*.

The *Drosophila* embryonic ventral nerve cord (VNC) harbors a bilateral set of 30 neuroblasts in each segment, each of which gives rise to a unique lineage of neural daughters. They undergo multiple rounds of asymmetric divisions that each produce a self-renewed neuroblast and a differentiating ganglion mother cell that divides once again to produce two postmitotic neural cells. As the neuroblast progenitors divide, they sequentially express a series of evolutionarily conserved transcription factors that specify cell fate of the neural progeny descended from each division (Allan and Thor, 2015; Brody and Odenwald, 2000; Doe, 2017; Elliott et al., 2008; Isshiki et al., 2001; Kohwi and Doe, 2013; Mattar et al., 2015; Miyares and Lee, 2019; Rossi et al., 2017; Telley et al., 2019). Hunchback (Hb), the first of such temporal identity factors, specifies the early cohort of neurons, called “early-born” neurons; these post-mitotic cells actively maintain *hb* transcription as a molecular marker of their early temporal birth (Figure 1a). Hb is normally expressed by neuroblasts for one or two divisions and is quickly repressed by a brief and transient pulse of its transcriptional repressor, seven-up (Svp) (Kanai et al., 2005). However, neuroblasts

remain competent to specify early-born identity neurons for several additional divisions, indicating that progenitor potential to specify particular cell fates persists for longer than the production of that cell type, a phenomenon observed in both insects and mammals (Cleary and Doe, 2006; Desai and McConnell, 2000; Kohwi et al., 2013; Pearson and Doe, 2003). This period of competence, which we refer to as the "early competence window," is thus a representation of the internal state of the progenitor, reflecting its potential to produce a specific cell type. This internal state can be experimentally observed by transgenically misexpressing Hb in the neuroblast and assessing whether the descendant neuron subsequently activates and sustains *hb* transcription endogenously, a key molecular characteristic of early-born identity. Note that misexpressed Hb in the neuroblast does not induce *hb* within the neuroblast itself, nor does misexpression directly in the post-mitotic neuron induce *hb* within the neuron. Only when Hb is supplied to the neuroblast during the early competence window does the postmitotic neuron that descends from that division activate endogenous Hb expression. Thus, the parental neuroblast "primes" the future transcriptional program that will be activated within the neuron, and once the early competence period ends, the neuroblast becomes refractory to Hb and can no longer specify early-born identity (Kohwi et al., 2013; Pearson and Doe, 2003). We previously showed that the early competence window closes when the *hb* genomic locus relocates to the nuclear lamina, a gene silencing hub (Shevelyov and Nurminsky, 2011; van Steensel and Belmont, 2017), in the neuroblast progenitor (Kohwi et al., 2013), and once this occurs, misexpressed Hb in the neuroblast no longer results in *hb* expression in the subsequent neuronal progeny. This change in *hb* gene positioning, which we observe as an increase in the fraction of *hb* genomic loci peripherally localized in neuroblast nuclei, occurs at mid-embryogenic stage 12, several divisions after *hb* has been transcriptionally repressed by a transient pulse of Svp (Figure 1b). Lamin loss-of-function mutants result in reduced peripheral localization of the *hb* gene and a concomitant extension in early competence, indicating a causal relationship between relocation and heritable *hb* gene silencing (Kohwi et al., 2013). Mechanisms that govern this second type of *hb* regulation through changes in gene positioning are not known.

Here we used the timed relocation of the endogenous, developmentally-regulated *hb* gene to the neuroblast nuclear lamina in intact *Drosophila* embryos to investigate mechanisms underlying genome architecture reorganization *in vivo*. We identify a hitherto undescribed, 250bp intronic DNA element (IE) necessary and sufficient for gene-lamina relocation. In isolation, the IE is sufficient to target a transcriptionally active reporter gene to the nuclear lamina and to silence

it. In contrast, removal of the IE from its endogenous locus has no effect on *hb's* normal transcriptional dynamics, but instead impairs *hb* gene relocation and extends progenitor competence to generate *hb*-expressing neurons. Thus, gene-lamina association in the progenitor can confer a heritably-silenced state refractory to activation in the neuronal progeny. Importantly, we identify the evolutionarily conserved Polycomb (PcG) chromatin factors act through this element to control *hb* gene-lamina interactions. Strikingly, we find that loss of PcG activity impairs *hb* gene-lamina relocation and extends neuroblast competence, without altering transcriptional dynamics, revealing an unexpected role in nuclear architecture. In sum, our results provide mechanistic insights into regulation of gene-lamina associations and progenitor competence transitions in intact animals.

Results

Chromatin profiling identifies a hb intronic DNA element that increases in accessibility upon lamina relocation

The neuroblast early competence window terminates when the key early-born neuron marker gene, *hb*, relocates to the neuroblasts' nuclear lamina, which disables it from transcriptional activation in the neural progeny. To generate hypotheses for possible mechanisms underlying *hb* gene repositioning in neuroblasts, we examined the chromatin structure at the *hb* genomic locus in neuroblasts before and after the *hb* gene becomes relocated to the nuclear lamina. We generated a transgenic fly line (*dpn-eGFP*) that expresses eGFP driven by an enhancer for the neuroblast-specific gene, *deadpan* (Dpn) (Awasaki et al., 2014) (Figure 1c and S1a) to purify precisely staged neuroblasts by fluorescence activated cell sorting (FACS) (Figure S1b,c). Neuroblasts were subjected to ATAC-seq to examine their chromatin accessibility profiles (Figures 1d and S1a). We bioinformatically validated the specificity of our data using the available *Drosophila* embryo single cell ATAC-seq (Cusanovich et al., 2018) and found strong correlation with the nervous system clusters (Figure S2b). Further, we found neural genes expressed in neuroblasts, such as *worniu* and *deadpan*, were associated with robust chromatin accessibility compared to non-neural genes (Figure S2c,d).

The *hb* gene's spatiotemporal expression pattern throughout embryonic development is well known. At stage 5, half of the embryo actively transcribes *hb*, and the *hb* gene body is highly accessible (Figure 1d), consistent with observations by others (Haines and Eisen, 2018). While *hb*

transcriptional enhancers (Hirono et al., 2012; McKay and Lieb, 2013) remained largely accessible at all stages, when the *hb* gene relocates to the nuclear lamina at stage 12, we found the gene body largely inaccessible; genes associated with the nuclear lamina are typically characterized by repressive features, including reduced chromatin accessibility (Milon et al., 2014; Pickersgill et al., 2006; Shevelyov and Nurminsky, 2011; van Steensel and Belmont, 2017). This decrease in accessibility is already partially apparent at stage 10, the earliest we are able to purify neuroblasts using the GFP reporter, despite active expression of Hb (Fig 1h); this perhaps indicates a change in chromatin state at the *hb* gene preceding the neuroblast transition to the Kruppel temporal window. Despite this, we found a region within the *hb* intron just downstream of the transcriptional start site that had increased in accessibility between stage 10 and 12 (p value = 0.0047) (Figure 1e), counter to a general trend that gene body regions tend to decrease in accessibility upon silencing (Milon et al., 2014).

The hb intron element is not required for proper hb transcription in the ventral nerve cord

To investigate whether the IE plays any role in *hb* transcriptional regulation in neuroblasts and/or its potential to be activated in neurons, we took advantage of a previously characterized transgenic line in which we integrated into the genome a bacterial artificial chromosome (BAC) containing the entire *hb* genomic locus. This 32kb BAC includes an hemagglutinin (HA) epitope tag fused to Hb ($Hb^{HA:WT}$), and we showed that $Hb^{HA:WT}$ faithfully reconstitutes endogenous Hb expression and function (Kohwi et al., 2013). Using this as a base, we used LoxP-mediated recombination to further selectively remove from the BAC ~250bp of the intron, corresponding to the ATAC peak, while preserving the splice sites (called "$hb^{HA:\Delta intron}$" Figure 1f). Both the wild type and the IE-deleted BAC transgenes were integrated into the same genomic locus using phiC31-mediated integration allowing direct comparison of the endogenously-expressed Hb^{HA} proteins.

Drosophila embryonic development is highly stereotyped, and gross morphological features unique to each developmental stage allow us to precisely compare Hb expression in stage-matched wild type and transgenic embryos. We found $hb^{HA:\Delta intron}$ embryos immunostained with anti-HA antibodies, which selectively detects Hb protein derived only from the $hb^{HA:\Delta intron}$ transgene, and anti-Hb antibodies, which detects Hb protein from both the native *hb* locus and the $hb^{HA:\Delta intron}$ transgene, show the same spatiotemporal pattern as in wild type embryos and embryos with the full length *hb* BAC (Figures 1g,h and S3a). In neuroblast 7-1 (NB7-1), one of the 30

neuroblasts that has a well-characterized lineage for which the even-skipped (Eve) transcription factor identifies its progeny, we detected HA and Hb in only the first two neurons, marking the early-born neuron fate, as is well-characterized in wild type embryos (Brody and Odenwald, 2000; Isshiki et al., 2001; Kohwi et al., 2013). Moreover, consistent with normal Hb expression dynamics in neuroblasts, we did not find extra early-born neurons that could have indicated extended neuroblast Hb expression. Thus, the 250bp *hb* IE does not play a role in regulating the normal Hb expression dynamics in the embryonic nerve cord.

The hb IE is required for hb gene relocation to the neuroblast nuclear lamina

We next investigated the consequence of the IE deletion on *hb* gene positioning. We mapped the physical position of the *hb* gene in neuroblast nuclei by DNA Fluorescence *in situ* hybridization (FISH) and 3D confocal imaging on whole embryos. Embryos were co-stained with Lamin Dm0, the Lamin B intermediate filament of the nuclear lamina, and Worniu, a pan-neuroblast marker. The *hb* DNA FISH probe targets a ~10kb region of the *hb* genomic locus and can detect the native *hb* gene as well as the 32kb BAC. We previously showed that the *hb* BAC, which contains *hb's* transcriptional enhancers and regulatory elements, behaves similarly to the native *hb* gene, including transcriptional regulation as well as the timing and frequency of gene relocation to the nuclear lamina, which reaches a plateau of ~50% (~60% are ≤0.04μm from lamin, "near") at stage 12 when the early competence window closes (Kohwi et al., 2013). The IE-deleted BAC was inserted in the same integration site, thus allowing a side-by-side comparison of the transgene positioning. In the $hb^{HA:\Delta intron}$ embryos, there are two endogenous *hb* gene loci and two *Δintron hb* loci, and thus, failure of the $hb^{HA:\Delta intron}$ gene locus to relocate to the neuroblast nuclear lamina would result in a concomitant decrease in the percentage of *hb* DNA FISH signals at the nuclear lamina at stage 12. Consistent with this prediction, at stage 12, 53.8±2.6% *hb* loci in $Hb^{HA:WT}$ neuroblasts compared to only 35.5±3.5% in $hb^{HA:\Delta intron}$ neuroblasts were at the lamina (P=0.002), and 62.9±2.7% of *hb* loci in $Hb^{HA:WT}$ neuroblasts compared to only 45.5±2.2% in $hb^{HA:\Delta intron}$ neuroblasts were within 0.04μm of the lamina (P=0.0009) (Figure 2a-c). The FISH probe can detect all four *hb* loci (Kohwi et al., 2013), but the images in the figure show a single z-plane of a representative neuroblast nucleus in which the center, brightest point of the DNA FISH signal can be seen. Results from older neuroblasts at stage 14 were similar: 56.6±7.2% of the *hb* loci were at the lamina in $hb^{HA:WT}$ neuroblasts compared to only 36.7+5.0% in $hb^{HA:\Delta intron}$ (P=0.007), and

65.8±4.5% *hb* loci were near the lamina in $hb^{HA:WT}$ compared to 50.3±5.3% in $hb^{HA:\Delta intron}$ neuroblasts (P<0.01). Together, the data show that while deletion of the IE does not impair normal *hb* transcriptional dynamics, the *hb* IE is required in the neuroblast for gene-lamina association.

The hb IE is required to terminate the neuroblast early competence window

hb gene relocation to the nuclear lamina occurs nearly synchronously across an otherwise heterogeneous group of neuroblasts at mid-embryogenic stage 12, terminating competence to specify early-born molecular identities. To investigate the biological consequence of deleting the IE in competence regulation, we focused on the NB7-1 lineage for which competence has been well-described (Cleary and Doe, 2006; Kohwi et al., 2013; Pearson and Doe, 2003). NB7-1 normally expressed Hb for two divisions and produces two Hb^+ U motoneurons (Figure 1a) but is competent to produce early-born neurons anytime within its first five divisions, as observed through both transient and continuous Hb misexpression (Meng et al., 2019; Pearson and Doe, 2003; Seroka and Doe, 2019). For our competence assay, we used the Gal4/UAS system (Brand and Perrimon, 1993) to drive continuous Hb misexpression in the neuroblast via the *UAS-hb* transgene and quantified early-born neurons molecularly identified by expression of Hb^{HA}, a proxy for endogenous *hb* transcriptional activation (Figure 2d-f). We used the *engrailed* (*en*)-gal4 driver, which drives strong expression in row 6 and 7 neuroblasts, including NB7-1 (Cleary and Doe, 2006; Kohwi et al., 2013; Pearson and Doe, 2003). Compared to $hb^{HA:WT}$, we found a pronounced increase in the number of HA^+ neurons produced in $hb^{HA:\Delta intron}$ flies (5.2 ± 1.3 neurons in $hb^{HA:WT}$ versus 12.7 ± 2.5 in $hb^{HA:\Delta intron}$, P<0.0001) (Figures 2e and S3b). $Hb^{HA:\Delta intron}$ cannot be induced by misexpression of Hb directly in the postmitotic neurons (Figure S4), just as for $Hb^{HA:WT}$ (Kohwi et al., 2013), arguing against the possibility that removing the IE reduces *hb* repression or lowers the activation threshold in response to Hb misexpression. We conclude that the *hb* IE functions as a regulatory element for the gene's relocation to the nuclear lamina, and this topological transition has an important biological consequence on progenitor competence.

The ~250bp hb IE is sufficient for nuclear lamina relocation and silencing of reporter gene driven by a constitutively active neuroblast enhancer.

To analyze how the *hb* IE functions when taken out of context of the endogenous genomic locus, we generated a neuroblast GFP reporter construct, in which its synthetic intervening sequence (IVS

intron) was swapped with the *hb* IE sequence. We implemented the ParS-ParB system (Saad et al., 2014) to compare the subnuclear positioning of the control *ParS-dpn-IVS-mCD4-GFP* construct versus one in which the IVS intron was replaced with either one or three tandem copies of the ~250bp *hb* IE, *ParS-dpn-1x(3x)hbintron-mCD4-GFP*. Briefly, a ParS sequence element inserted into the reporter transgene recruits mNeon-fused ParB proteins (Figure 3a), allowing fluorescent visualization of the transgene locus within the nucleus (Figure 3b). Both the control and the IE-swapped constructs were inserted into the identical genomic locus for direct comparison *in situ*. In the *ParS-dpn-IVS-mCD4-GFP* control fly line, we found 21.6$\pm$2.6% loci at the lamina and 30.7$\pm$2.3% loci near ($\leq$0.4μm) the lamina in stage 14 neuroblasts (297 loci quantified from N=3 embryos), consistent with observations from others that the genome is non-static (Kind et al., 2014), and even non-LADs (lamina associated domains) can be peripherally localized ~30% of the time (Guelen et al., 2008; Harr et al., 2015; Zullo et al., 2012). In contrast to the control, in the *ParS-dpn-1xhbintron-mCD4-GFP* fly line we found 46.7$\pm$1.5% loci at or 59.4$\pm$5.3% near the lamina (304 loci quantified from 3 embryos), and in *ParS-dpn-3xhbintron-mCD4-GFP* fly line we found 53.5$\pm$2.8% loci at or 62.7$\pm$3.2% near the lamina (494 loci quantified from N=4embryos), a significant increase in localization at the nuclear lamina (Figure 3c) compared to the control transgene, despite being driven by a constitutively active neuroblast enhancer. Thus, the *hb* IE is both necessary and sufficient for gene-lamina relocation *in vivo*.

The *ParS-dpn-IVS-mCD4-GFP* control reporter line expresses GFP in the neuroblasts of the VNC and is detectable from stage 10. However, in the *ParS-dpn-3xhbintron-mCD4-GFP* embryos, GFP is silenced and never detectable in the neuroblast at any stage, even after allowing time for GFP accumulation in the neuroblast and imaging with ten times the laser power as used for the control reporter line (5.5% versus 0.5%, respectively) (Figure 3d,e). In *ParS-dpn-1xhbintron-mCD4-GFP* embryo, GFP signal was also severely reduced, but became visually detectable by stage 14, indicating a dosage effect of the *hb* intron element replacement and the sufficiency for even one copy of the *hb* intron element to nearly fully silence an otherwise transcriptionally active GFP transgene (Figure 3e). The silencing of the transgene with only ~60% localization at the lamina likely reflects the mobility of the genome. Indeed, live-imaging studies have shown confined diffusion of LADs (Bronshtein et al., 2016; Qin et al., 2017). Such dynamics cannot be fully captured in fixed embryo preparations, in which we observe only a snapshot of the genome at a time and likely underestimate the fraction of gene loci functionally associated with

the lamina. As the peripheral localization and transcriptional silencing are coincident, it is difficult to determine whether the reporter transgene silencing was the cause or consequence of relocation to the lamina. However, our observations are consistent with others' that relocation to the lamina can silence transcriptionally active reporter genes (Finlan et al., 2008; Reddy et al., 2008), and importantly, in the biological context of the endogenous *hb* gene, in which transcriptional repression occurs significantly prior to lamina relocation (several divisions in NB7-1), removal of the IE blocks lamina-relocation without disrupting transcriptional dynamics. Thus, the data show that lamina-association can serve a function different from transcriptional repression, to confer a heritable, refractory gene state that blocks activation in descendent neurons born after mitotic divisions.

The Polycomb (PcG) chromatin factors target the hb IE

Though subnuclear repositioning of genes is an important component of gene regulation and has been observed across multiple animal models (Kohwi et al., 2013; Meister et al., 2010; Peric-Hupkes et al., 2010; Williams et al., 2006), proteins that recognize specific gene elements to facilitate relocation are not known. Given the increase in chromatin accessibility of the *hb* intronic element at the stage when the gene relocates to the neuroblast nuclear periphery for silencing, we hypothesized the IE may be a binding target for a protein(s) mediating gene relocation. We identified two juxtaposing putative binding motifs for Pho, the PcG subunit with a sequence-specific DNA-binding domain (Brown et al., 2018; Oktaba et al., 2008) (Figure 4a) coinciding with the dip in reads at the ATAC-seq peak, a typical profile for a chromatin accessible site in which bound proteins interfere with Tn5 transposition at that position (Bentsen et al., 2020; Buenrostro et al., 2013; Hesselberth et al., 2009). PcG proteins are chromatin factors well known for their important role in the epigenetic regulation of developmental genes through the cooperative activity of two multimeric protein complexes, Polycomb Repressive Complex 1 (PRC1) and PRC2, which are recruited to chromatin through different paths (Beuchle et al., 2001; Grossniklaus and Paro, 2014; Negre et al., 2006; Papp and Muller, 2006; Schuettengruber and Cavalli, 2009; Schwartz et al., 2006; Struhl, 1981; Tolhuis et al., 2006). By immunostaining for Posterior Sex Combs (Psc) and Enhancer of Zeste [*E(z)*], the core subunits of PRC1 and PRC2, respectively, we found that both are enriched in embryonic neuroblasts (Figure 4b). Taking advantage of available *Drosophila* ChIP-seq data sets from larval brain and whole embryo (Bonnet

et al., 2019; Brown et al., 2018), we identified strong ChIP enrichment of both PRC1 and PRC2 subunits across the *hb* genomic region of ~25kb, with robust binding of multiple subunits directly aligning at the *hb* intron site (Figure 4c). Interestingly, putative Hb target genes in the CNS (Sen et al., 2019) are significantly enriched for chromatin accessible Pho sites like the *hb* intron, compared to non-Hb targets across the genome, (Figure S5). Although *hb* is the only known universal marker of early-born neurons, which consist of diverse cell types, perhaps genes associated with early-born identity similarly become refractory to activation in neurons at the end of the neuroblast's early competence window.

PRC1 is required for hb gene relocation to the neuroblast nuclear lamina but not for hb repression

To test whether PcG factors are required for *hb* gene-lamina relocation, we examined neuroblast *hb* gene positioning in Posterior sex combs (Psc) loss of function mutants. Psc is central to PRC1 repressive activity and plays a primary role in gene silencing (King et al., 2005). We found that Psc^{h27} null neuroblasts showed a significant reduction in *hb* loci at the nuclear lamina (Stage 12: 53.4±4.3% in wild type versus 26.7±5.7% in $Psc^{-/-}$, P=0.001; Stage 14: 57.1±7.9% in wild type versus 32.2±5.5% in $Psc^{-/-}$, P=0.01) (Figure 5a). Thus, PRC1 is required for *hb* gene-lamina association.

PcG proteins are critical players in stabilizing cell type specific gene expression programs by maintaining gene repression. Given that actively transcribed genes are often localized away from the repressive nuclear periphery (Meister et al., 2010; Peric-Hupkes and van Steensel, 2010), one possible explanation for reduced *hb* gene-lamina association could be that *hb* becomes de-repressed in *Psc* mutant neuroblasts. Surprisingly, we found no differences in Hb spatiotemporal expression in Psc^{e24} or $E(z)^{731}$ loss of function mutant neuroblasts; Hb was expressed in newly formed neuroblasts and rapidly downregulated with the same timing as in wild type (Figure 5b,c). Importantly, we did not observe any Hb de-repression in neuroblasts of older mutant embryos at stage 15.

To address the possibility of maternal effects that could mask zygotic mutant phenotypes, we examined a maternal and zygotic loss of function mutants for extra sex combs ($esc^{mat\text{-}zyg\text{-}}$) (Struhl, 1981; Tie et al., 1998), a component of PRC2 essential for E(z) methyltransferase activity (Bonnet et al., 2019). Though $esc^{mat\text{-}zyg\text{-}}$ mutants show strong de-repression of its Hox target, Abdominal B, we did not find Hb de-repression even in late-stage neuroblasts (Figure S6a,b). We

also examined a zygotic double mutant for Psc and Su(z)2 (Psc^{P3C}), which has a severe PRC1 loss of function phenotype (Classen et al., 2009). Similar to $esc^{mat\text{-}zyg\text{-}}$ mutants, Psc^{P3C} also showed Abdominal B de-repression across the animal by mid-embryogenesis but no de-repression of Hb in late stage mutant neuroblasts. Further supporting the lack of PcG-mediated repression of *hb* in neuroblasts, in wild type embryos, we find markedly low levels of histone H3 Lysine 27 trimethylation (H3K27me3) H3K27me3, the primary histone modification associated with PcG-mediated gene silencing, in neuroblasts compared to neighboring cells (Figure S6c). Histone H3 as well as both PRC1 and PRC2 components, however, are readily detectable in neuroblasts (Figures S6c and 4b), and loss of PcG results in a reduction in *hb* relocation to the nuclear lamina and an extension in early competence. Together, the data show that in neuroblasts, PcG activity is required for *hb* gene lamina relocation but not *hb* repression.

PcG chromatin factors are required to terminate the early competence window

Given the effects of PcG loss on *hb* gene positioning, we next tested PcG proteins in neuroblast competence using our competence assay on NB7-1 (Figures 6 and S7a,b). We found an extension in the early competence window in Psc^{h27} null mutants (4.5±2.3 $Hb^{HA+}Eve^{+}$ neurons in wild type compared to 7.2±2.0 in Psc^{h27}, P<0.0001), and phenotypes were consistent with a different *Psc* null allele (Psc^{e24}, 8.6±2.5 $Hb^{HA+}Eve^{+}$ neurons, P<0.0001). Similarly, we found that the early competence window was extended in *E(z)* mutants. Compared to wild type (5.3±1.2 $Hb^{HA+}Eve^{+}$ neurons), $E(z)^{731}$ mutants had an extended early competence window (8.7±2.7 in $E(z)^{-/-}$, P<0.0001). *E(z)* heterozygous embryos had a small, but statistically significant increase in $Hb^{HA+}Eve^{+}$ neurons as well (6.3±1.6 in $E(z)^{+/-}$, P=0.0006). Together, we show that either loss of PcG or deletion of the 250bp IE containing the PcG-binding site disrupts *hb* gene relocation to the neuroblast nuclear lamina and a failure in the timely closure of the early competence window. However, in both cases, normal *hb* transcriptional dynamics are not compromised, indicating that gene-lamina interactions and transcriptional regulation can be controlled separately, and that in neuroblasts PcG can play a unique role in nuclear architecture, by regulating gene-lamina association (Figure 7).

Discussion

While changes in nuclear architecture has increasingly become a major focus of understanding gene regulation during development, how genome reorganization is controlled and how those

changes influence subsequent cell fate decisions *in vivo* are not known. To address this challenging question, we took advantage of the *Drosophila* embryo neuroblast model system in which we had previously documented the *in vivo* developmentally-timed relocation of the *hb* gene to the nuclear lamina *in vivo*. This relocation, a critical step in terminating neuroblast competence to generate neurons of early-born identity, indicates that the underlying genome architecture of the progenitor determines the transcriptional identity of the descendent neuron. Here, we identified a hitherto uncharacterized core 250bp genomic element within the *hb* intronic DNA sequence that is required for this topological relocation, without affecting the gene's normal transcriptional dynamics within the neuroblast. Upon deletion of this element, the *hb* gene fails to relocate to the lamina, extending neuroblast competence to produce *hb*-expressing neurons. Thus, the IE does not directly regulate *hb* transcription *per se*. Rather, the potential for *hb* expression in neurons, and consequently neuronal identity, is established by the subnuclear *hb* gene positioning within the progenitor, and this topological organization is regulated by the IE.

The *hb* IE in isolation, however, is sufficient to reposition a reporter gene driven by a constitutively active enhancer to the nuclear lamina and can repress it *in vivo*. Thus, by examining its function in both an artificial reporter context as well as in its endogenous context of a developmentally-regulated gene in intact animals, we demonstrate this genomic element is responsible for gene-lamina association. However, the biological consequence of this element – transcriptional repression versus heritably-refractory gene state – depends on the specific genomic context. The fact that *hb* gene-lamina association in the progenitor affects the *hb* gene state in the neuron indicates that changes in nuclear architecture can have functional consequences in cells born after multiple mitotic divisions.

Identification of the *hb* intron as a core regulatory element led to our findings that PcG chromatin factors are key regulators of gene-lamina interactions. In both *Drosophila* and mammalian cells PcG proteins have been shown to engage in long-range interactions to facilitate repression (Bantignies et al., 2011; Bonev et al., 2017; Eagen et al., 2017; Gentile et al., 2019; Gozalo et al., 2020; Kundu et al., 2017; Tolhuis et al., 2011), and loss of PRC1 was shown to lead to Hox gene decompaction prior to de-repression (Cheutin and Cavalli, 2018). Thus, PcG function in higher order genome architecture has been intimately tied to its role as a developmental repressor. Whether PcG proteins have a repression-independent function in regulating genome architecture is an important and emerging question with very few *in vivo* studies. In murine

embryonic stem (ES) cells, loss of PRC2 or PRC1-mediated chromatin interactions is not necessarily accompanied by gene activation (Boyle et al., 2020; Cruz-Molina et al., 2017), suggesting that PcG factors might regulate a subset of target genes at the level of higher order chromatin architecture without affecting their repressive state. However, determining whether such regulation is biologically meaningful requires careful validation in tissue context. We find that in neuroblasts neither loss of PRC2 or PRC1 results in de-repression of Hb in neuroblasts once its normal expression window ends, even upon loss of both maternal and zygotic *esc*, the most severe genetic loss of PRC2 function that causes genome-wide loss of H3K27me3 deposition (Bonnet et al., 2019). This is further supported by our observations that neuroblasts have markedly lower H3K27me3 signals compared to their neighboring cells. Thus, while maintenance of *hb* repression once it is silenced in neuroblasts does not appear to rely on PcG proteins or H3K27me3 chromatin modifications, PcG activity is essential for *hb* gene-lamina association.

Furthermore, in the context of the developing animal, we found that the PcG-mediated gene-lamina association of the *hb* gene plays an essential role in regulating neuroblast competence to specify early-born fate neurons. Investigating mechanisms controlling stem/progenitor competence is crucial to understanding how specific cell fates are established in an organized, coordinated manner within the developing brain. PcG function has been implicated in stem cell competence in many animal systems, but mechanisms remain largely unknown. Upon removal of PRC2, germ cells in *C. elegans* become competent to respond to terminal selector transcription factors and directly convert to specific neuronal cell types (Patel et al., 2012). Loss of PcG activity has been shown to extend *Drosophila* neuroblast competence to respond to the temporal identity factor Kruppel (Touma et al., 2012). During the neurogenesis-to-gliogenesis transition in mouse, loss of a PRC1 subunit, Ring1B, leads to an increase in progenitor competence to respond to Wnt signaling to induce neurogenesis (Hirabayashi et al., 2009). In murine ES cells, loss of PRC2 reduces competence to activate anterior neural genes in response to differentiation (Cruz-Molina et al., 2017). Thus, PcG protein function in neural competence is likely highly conserved, underscoring the importance of understanding the mechanisms of their function *in vivo*.

In summary, our results provide important mechanistic insights into nuclear architecture reorganization *in vivo* by identifying a small genomic element responsible for gene-lamina association of a developmentally-regulated gene. We identified PcG chromatin factors as key

regulators that associate with this gene element for lamina relocation without affecting the gene's transcriptional dynamics, demonstrating a non-canonical role in nuclear architecture. Importantly, we provide functional evidence that topology-specific gene regulation plays a critical role *in vivo*, to control neuroblast early competence. Competence transitions are an important developmental feature of neural progenitors that not only determine the timeframe when each neural cell type can be generated during development, but provide the heritable blueprint upon which the transcriptional program of the descendent neurons is executed. Future work will elucidate whether similar processes are employed during mammalian neurogenesis and how such mechanisms have contributed to the evolution of neural diversity.

Limitations of the study: While our results show that the IE and PcG proteins are required for *hb* gene relocation to the neuroblast nuclear lamina to confer a heritably-silenced gene state, there may be additional factors that play a role in establishing and/or maintaining *hb* association with the nuclear periphery. Deletion of the IE results in a greater extension in early competence compared to loss of Psc or E(z), which could be due to compensatory function between PcG subunits, but also yet unknown factors that target the IE. Furthermore, we do not have the full picture of PcG function within embryonic neuroblasts. For the *hb* gene, we have shown that PcG function is required for its relocation to the nuclear lamina and not for its repression, but further studies will be required to determine whether PcG in neuroblasts regulates gene-lamina interactions across the genome, and the extent to which such interactions are also decoupled from the repressive functions for which PcG proteins are well known. PcG has been associated with maintenance of gene repression through catalyzing H3K27me3 histone marks, and these marks have also been proposed to prevent spreading of repression beyond LAD borders (Harr et al., 2015; Guelen et al., 2008). However, given the dearth in H3K27me3 signals in neuroblasts compared to other cell types, and the lack of repressive effects that loss of E(z) and esc has on *hb*, it would be fascinating and important to map H3K27me3 deposition in neuroblasts and determine the functional relationship between PcG proteins and H3K27me3 in the context of nuclear architecture.

Acknowledgements:

We greatly thank Drs. Gary Struhl and Stavros Lomvardas for critical scientific discussion and feedback on the manuscript. We thank Dr. Jürg Müller on discussion on PcG biology. We additionally thank Drs. Hynek Wichterle, Steve Siegelbaum, Wes Grueber, Carol Mason, Chris Q. Doe, Rui Galvão, and Raphaelle Laureau for comments on the manuscript. We thank members of the Kohwi lab, especially Daiki Tagami and Sofiya Patra, for technical assistance with experiments. MK received support from NIH grants R00HD072035 and HD092381, Rita Allen Foundation, and Whitehall Foundation. TL received support from the NYSTEM training grant. HZ received support from Columbia University's Science Research Fellows Program.

Author contributions:

TH, TL, and MK designed and executed the experiments, analyzed the data, and wrote the manuscript. HZ and NM assisted with all experimental planning, execution and data analysis.

Declaration of Interests:

The authors declare no competing interests.

Main Figure Titles and Legends:

Figure 1: Chromatin accessible *hb* intronic element does not regulate *hb* transcription.

a, Neuroblast 7-1 (NB7-1, center) and its neural lineage arranged by birth order. **b,** over time, *hunchback* (*hb*) gene in the neuroblast is transcriptionally repressed (1) then relocates to the nuclear lamina (2), closing the early competence window. **c,** schematic of neuroblast purification. **d**, ATAC-seq profiles of stage 5, 10 and stage 12 neuroblasts (st10 and st12 traces are an average of N=5 and 4 replicates, respectively). Black horizontal bars indicate known *hb* transcriptional enhancers/promoters (Hirono et al., 2012; McKay and Lieb, 2013). Red arrow, *hb* intronic element. ***e***, log2 ratio. **f,** Schematic of IE deletion from the 32kb *hb* genomic BAC and generation of transgenic animals. **g,** Schematic of ventral and lateral views of the embryonic VNC; neurons (blue), neuroblast (purple). **h,** Ventral views of wild type and $Hb^{HA:\Delta intron}$ embryo VNC immunostained with anti-Hb (all Hb protein), anti-HA (BAC-specific), and anti-Dpn (pan-neuroblast) antibodies. Bottom panels show NB7-1's U motoneuron (Eve^{+}) neural progeny; inset shows neurons from different z planes. See also Figures S1 and S2.

Figure 2: The *hb* intron is required for gene relocation the nuclear lamina and termination of the early competence window.

a, Single z-plane showing DNA FISH signal of representative neuroblast nuclei. Whole stage 12 and 14, $Hb^{HA:WT}$ or $Hb^{HA:\Delta intron}$ embryos were hybridized with *hb* DNA probe and immunostained for Lamin Dm0 and pan-neuroblast marker, Worniu. **b,** fraction of *hb* loci at neuroblast nuclear lamina (N=3 embryos per genotype, loci quantified shown on each bar). **c**, Spatial distribution of *hb* loci binned by gene-lamina distances. **d,** NB7-1 lineage early competence assay in $Hb^{HA:\Delta intron}$ vs $Hb^{HA:WT}$ (*en>GAL4, UAShb*). **e,** Quantification of early competence window ($Eve^{+}HA^{+}$) and total lineage length (Eve^{+}). **f,** Schematic summary of early competence window in $hb^{HA:\Delta intron}$ neuroblasts. All data are represented as mean ± SD. See also Figure S3 and S4.

Figure 3: The *hb* intronic element is sufficient to relocate a GFP reporter gene to the neuroblast nuclear lamina.

a, Schematic of genotypes. **b,** *In situ* detection of reporter transgene in whole, stage 14 embryo neuroblasts. Representative image of single z-plane of neuroblast showing ParB-Neon (transgene locus) and lamin from either IVS control (top panels) or *hb* intron-swapped reporter constructs. **c,** quantification of transgene loci localized at or near the lamina. **d**, Ventral views of 50-micron z projections through the neuroblast layer of control, 1x intron-swapped, 3x intron-swapped GFP reporter embryos showing dose-dependent effects of the *hb* intron element insertion. Embryos are stained with GFP, Dpn (pan-neuroblast) and DAPI. **e,** Neuroblast GFP signal quantified as a ratio of neuroblasts to background. Each N is average of 50 neuroblasts. All data are represented as mean ± SD.

Figure 4: Chromatin profiling reveals highly-accessible PcG-binding site in *hb* intron.

a, ATAC-seq signal (green) at the *hb* locus shown at two scales. Two putative Pho binding motifs indicated in red; respective position Weight Matrix within *hb* intron ATAC peak are shown below. **b,** VNC of stage 12 embryos showing Psc or E(z) (green), pan-neuroblast markers, Dpn, Wor (magenta). **c,** ChIP-seq profiles of PRC1 and PRC2 subunits across ~25kb *hb* genomic region (gray**)** aligned with stage 12 neuroblast-specific ATAC-seq data (green). ChIP-seq

profiles (Brown et al., 2018); last Pho ChIP-seq profile (Bonnet et al., 2019). Red/Black bars, statistically significant putative Pho binding motifs (red bars, inverse of p-value < Q1 + 1.5*IQR). Normalized ChIP (log2 ChIP/input ratio, gray lines) peaks directly align with the ATAC signal (RPM normalized, green line) peak at the Pho motif site (center dashed line). See also Figure S5.

Figure 5: PRC1 is required for *hb* relocation to nuclear lamina in neuroblasts, but not in *hb* repression.

a, *left:* single z-plane of DNA FISH image of representative neuroblast nuclei from intact stage 12 and 14, WT or $Psc^{-/-}$ embryos. *Right*: fraction of *hb* loci at or near neuroblast nuclear lamina (N=3 embryos per genotype; quantified loci shown on each bar). **b,** Ventral view of stage 12 and 15 VNC from WT, $Psc^{-/-}$ and $E(z)^{-/-}$ embryos immunostained for Hb and Dpn. At late stage 12, Hb^{+} neuroblasts detected only in thoracic segments (arrows); no Hb^{+} neuroblasts detected in abdominal segments (*). (midline, solid lines). **c,** Proportion of Hb^{+} neuroblasts in $Psc^{-/-}$ or $E(z)^{-/-}$ embryos (N=3). All data are represented as mean ± SD; *ns* = not significant. See also Figure S6.

Figure 6: PcG chromatin factors are required to terminate the early competence window.

a, Early competence assay comparing WT to Psc^{h27} or $E(z)^{731}$ embryos. Dotted circles indicate early-born neurons of NB7-1 lineage. Insets show neural progeny from overlapping z planes. Quantification shown at the right. **b,** schematic summary of results. All data are represented as mean ± SD. See also Figure S7.

Figure 7: Summary model. Cis-acting, 250bp intronic element regulates *hb* gene relocation to the neuroblast nuclear lamina in mid-embryonic neuroblasts. The intronic element is bound by PcG chromatin factors which are required for *hb* gene relocation. Schematic to the right shows early competence window of each genotype. *Bottom*, *hb* intron element is sufficient to relocate GFP reporter construct to nuclear lamina and silence it. Gray box highlights the gene positioning phenotypes of each genotype.

STAR methods

RESOURCE AVAILABILITY

Lead Contact

Further information and requests for resources and reagents should be directed to and will be fulfilled by the Lead Contact, Minoree Kohwi (mk3632@columbia.edu).

Materials availability

Drosophila stocks and other reagents from in this study are available upon request from the Lead Contact, Minoree Kohwi, or from public/commercial sources that are listed in Key Resources.

Data and Code availability

The ATAC sequence data reported in this paper have been deposited to the NCBI Sequence Read Archive with the accession number PRJNA754600 (https://www.ncbi.nlm.nih.gov/bioproject/PRJNA754600). Any additional information required to reanalyze the data reported in this manuscript will available from the Lead Contact upon request.

EXPERIMENTAL MODEL AND SUBJECT DETAILS

Fly Lines

Wild-type *(w1118)*, Psc^{h27} (Bloomington, BL#5547), Psc^{e24} (BL #24155), $E(z)^{731}$ (BL #24470), *1407-GAL4* (BL #8751), *CQ2-GAL4* (BL #7466), *en-GAL4 (chrom III,* BL #46438), *en-GAL4* (chrom II, (Harrison et al., 1995; Isshiki et al., 2001), *UAS-hb* (Wimmer et al., 2000), esc^{6} and esc^{5} (Struhl, 1981; Tie et al., 1998), $Psc\text{-}Su(z)2^{P3C}$ (*P3C*) (Classen et al., 2009), $hb^{HA:WT}$ (Kohwi et al., 2013). Flies were raised on a standard cornmeal/molasses medium at 25C.

METHOD DETAILS

Plasmids and BAC

To generate *dpn-eGFP* was generated in this study by modifying a *dpn-GAL80* construct (kind gift from Chris Doe) to replace *GAL80* with *eGFP* (Addgene #1299) and was inserted into *attP2*

and *attP40* integration sites. $hb^{HA:\Delta intron}$ was generated by using recombineering (Venken et al., 2009) to remove a portion of the *hb* intron from a 32kb BAC containing the *hb* gene locus with an N-terminal HA epitope tag (Kohwi et al., 2013). *ParS-dpn-1xhbintron-mCD4-tdGFP* and *ParS-dpn-3xhbintron-mCD4-tdGFP* were generated by replacing the*10XUAS* and *GFP* of the *pJFRC81-10XUAS-IVS-Syn21-GFP-p10* (pJFRC81) (Addgene #36432), *with dpn* (from the *dpn-gal80* construct, above) and *mCD4* (BL #35836), and then subsequently replacing the *IVS* intron with either a single copy, or three tandem copies of the 250bp element of the *hb* intron. The ParS sequence from cloned from pFG4-INT2. The *dpn-ParB-Neon2* construct was generated from the pBPGUw-attB (Addgene #17575). ParB-Neon sequence from an hsp70-ParB-Neon plasmid was cloned into an intermediate plasmid containing the Dpn enhancer followed by the Drosophila Synthetic Core Promoter (DSCP) and terminated by the 3'UTR of hsp70. Both pFG4-INT2 and hsp70-ParB-Neon plasmids were a kind gift from Dr. Richard Mann. All transgenes above were generated using Sequence Ligation Independent Cloning (SLIC)(Jeong et al., 2012). To generate the Δ*intron:HA:hb* construct, we synthesized primers (below) with 80nt homology to sequences flanking the *hb* intron to amplify a *lox* flanked Kanamycin resistance (KanR) cassette within the PL-452 N-eGFP plasmid. This fragment was used to recombiner the 32kb *HA:hb* BAC^{ampR}, which replaced 246bp of the intron with 86bp sequence from the PL-452N-eGFP plasmid. The final construct was inserted at attp2 (3L 68A4) using site specific integration.

5'HR Forward: tcatgatctttataatcaccgtcatggtctttgtagtccatcttggcggctctagacggctgtaatggataagaaaacag agagagtggggttagtctcggcatggacgagctgtacaag; 3'HR Reverse:

ataatatacttgcaaatccttacgaaaatcccgacaa

atttggaatatacttcgatacaatcgcaatcatacgcactgagcggccacgaaacggtctagtggatcccctcgagggaccta.

Cell dissociation and FACS

dpn-eGFP embryos were collected for one hour, dechorionated, and immersed in halocarbon oil (Sigma-Aldrich) to identify stage. For stage 5 ATAC-seq, five embryos were collected after aging for one hour at 25°C, dissociated and directly processed for ATAC-seq. For stage 10 and 12 neuroblasts, embryos older than stage 4 were removed by hand to ensure developmental stage uniformity. Embryos were then aged at 18°C for 16 hours to reach stage 12, or at 29°C for 3 hours to reach stage 10 before dissociating in Chan and Gehring's Balanced Saline (C&G) buffer (Chan and Gehring, 1971) with 2% fetal bovine serum. Cells were incubated with Calcein Violet

450 AM and 7-AAD (Thermo Fisher Scientific) to label live and dead cells, respectively, and sorted on a Beckman Coulter MoFlo Astrios EQ (Fig. S3B). FACS based on their viability, size, granularity and GFP fluorescence intensity (Fig. S3C). Neuroblasts were collected into cold ATAC-seq lysis buffer and incubated for 10 min on ice prior to transposition. A fraction of sorted cells were plated on glass coverslips and fixed for 15min at room temperature in 4% formaldehyde for immunostaining (Fig. S3D). FACS gates were adjusted to include the large, round neuroblasts and eliminate $Elav^{+}$ neurons that formed neuroblast-sized clusters. During each FACS, cells were examined under brightfield to confirm these criteria.

Low input ATAC-seq

ATAC-seq was performed as described in (Buenrostro et al., 2015) with minor modifications for low-input. After sorting, the transposition reaction mix (13.5µl 2x TD Buffer + 1.5µl Tn5 Transposase, Tn5 Illumina) was added to neuroblasts and incubated for 30min at 37^{o}C. ATAC-seq libraries were generated using NEB Next High Fidelity 2xPCR Master Mix to amplify transposed DNA using barcoded primers (Buenrostro et al., 2013). Concentrations and fragment size distributions were checked on a 2100 Bioanalyzer. Libraries were pooled and sequenced paired-end on an Illumina NextSeq500 sequencer. Four biological replicates of neuroblasts were sequenced. Paired-end sequencing data were aligned to the Dm6 *Drosophila* genome using bowtie2. PCR duplicates were removed and read positions relative to Tn5 cut site were adjusted as in (Buenrostro et al., 2013). For visualization purposes, all samples were normalized by Reads per million (RPM). Peaks were called using MACS2 from <100bp fragment pairs representing open regions and ranked by fold change.

ATAC-seq data processing

Raw sequencing data (basecall files (BCLs)) were converted to FASTQ format using bcl2fastq conversion software (Illumina). Quality assurance was performed using FASTQC (S. Andrews 2010). Adaptor sequences were removed using cutadapt in paired-end mode (-m5 -e 0.2 -o {R1} -p {R2}) (Martin, 2011). Paired-end reads were aligned against dm6 (dmel_r6, Flybase) using bowtie2 (-k 4 -X2000 --local --mm) (Langmead and Salzberg, 2012). PCR duplicate were remove using Picard MarkDuplicatesReads (Picard Toolkit, Broad Institute) and further filtering was done using samtools (-F 1804 -f 2 -q 30 chrX chrY chr4 chr2L chr2R chr3L chr3R) (Li et

al., 2009). Read positions were adjusted as in (Buenrostro et al., 2013) on bedgraph file using +5/-4 bp shift for first in pair and second in pair respectively and read per million (RPM) normalization was applied to all samples using BEDTools genomecov (-scale {RPM} -d) (Quinlan and Hall, 2010) before generating bigwig file for visualization using bedGraphToBigWig (Kent et al., 2010).

Peak detection for ATAC-seq data and differential analysis

Peaks were called from fragment-size filtered bam files (< 100bp, representing open region only) using MACS2 (callpeak -f BAMPE -g dm -q 1.10^{-6} --slocal 10000 --nomodel --shift -100 --extsize 200 --nolambda) (Zhang et al., 2008). Peaks were ranked using their MACS2 fold change and the top 20% were analyzed for association with neural genes. Replicates were correlated with single cell ATAC data (Cusanovich et al., 2018)by extracting bigwig tracks from their scATAC-seq browser and running plotCorrelation from deepTools (Ramirez et al., 2016). Differential analysis for ATACseq peaks at Stage 10 vs. Stage 12 were performed using DiffBind (Ross-Innes et al., 2012) (all aligned file replicates were used along with their specific peak list). We used 0.05 as threshold of significance for differential analysis results.

Immunohistochemistry

Embryos were immunostained following standard protocols (Rothwell, 2000). Briefly, embryos were fixed in a 1:1 mixture of 4% formaldehyde in PEM buffer (0.1M Pipes, 1mM $MgS0_4$, 2mM EGTA) and N-heptane and rocked for 22 min at room temperature. Embryos were devitellinized by vigorous shaking in a 1:1 mixture of methanol:heptane and washed with PBS before staining. Embryos were incubated in primary antibodies diluted in PBS-0.1% Tween 20 (PBT) overnight at 4^oC, secondary antibodies at room temperature for 1.5hrs, and streptavidin for 20min at room temperature.

Immuno-DNA FISH

We performed DNA *in situ* hybridization (DNA-FISH) as previously described (Bantignies et al., 2011; Kohwi et al., 2013). Briefly, embryos were fixed in 4% formaldehyde in PIPES buffer (60mM KCl, 15mM NaCl, 0.5mM spermidine, 0.15mM spermine, 2mM EDTA, 0.5mM EGTA, 15mM PIPES pH 7.4) and rocked for 25 min at room temperature with an equal volume of heptane,

649 followed by vigorous shaking in a 1:1 mixture of methanol:heptane to release the embryos
650 (methanol cracking). We made the *hb* DNA FISH probe by amplifying genomic DNA spanning
651 a ~10kb region at the *hb* locus using PCR (Table S1) and generated fluorescent probes using the
652 DNA FISH Tag kit (Thermo Fisher Scientific). Rehydrated embryos were treated with RNaseA
653 (150mg/ml) for 2hr at room temperature and washed 1hr in PB-0.3%Triton-X (PBTx). Embryos
654 were gradually stepped into 100% pre-hybridization mixture (pHM: 50% formamide; 4XSSC; 100
655 mM NaH2PO4, pH 7.0; 0.1% Tween 20) by a series of PBTx:pHM washes for 20min each.
656 Embryos were pre-hybridized 1h at 37ºC, denatured 15min at 80ºC and rocked 16h at 37ºC in
657 FISH DNA hybridization buffer (10% Dextran sulfate, 50% deionized formamide, 2XSSC, 0.5
658 mg/ml Salmon Sperm DNA) containing denatured probe. Embryos were washed in a series of
659 decreasing formamide/0.3% CHAPS solutions at 37ºC with final washes at room temperature.
660 Embryos were subsequently immunostained according to standard immunochemistry protocol,
661 mounted in vectashield (Vectorlabs) and imaged on a confocal microscope, Zeiss LSM 700.
662
663 **Confocal imaging**
664 3D imaging was done on a Zeiss 700 Axio Imager 2 laser scanning confocal. DNA-FISH and
665 ParB-ParS images were taken at a 0.4µm step size, and pinholes were adjusted to have equal
666 optical section thickness for all channels.
667
668 **QUANTIFICATION AND STATISTICAL ANALYSIS**
669 **Image analysis**
670 All image analyses were done on Fiji (Schindelin et al., 2012). For DNA-FISH, we identified the
671 z-plane in which the FISH signal was strongest and measured the shortest distance to the nuclear
672 lamina. FISH signals for which pixels overlapped with those of lamin signal was scored to be
673 "on" lamin, and FISH foci not touching lamin but still within 0.4µm of the lamina was scored as
674 "near." Embryos were scored twice by two independent observers.
675
676 **ChIP-seq analysis**
677 Raw ChIP-seq datasets from Brown et, al. 2018 (GSE102339) (Brown et al., 2018) for E(z), Pc,
678 Ph, Psc, Pho and input and Bonnet et, al. 2019 (GSE114832) (Bonnet et al., 2019) for Pho and
679 input were processed as follows: adaptor removal using Cutadapt (-m 5, -e 0.2), alignment to

dm6 using bowtie2 (-local, --very-sensitive-local), removal of PCR duplicates using PICARD Mark duplicates, removal of mitochondrial DNA and read quality filter at 30 using Samtools (-q 30). Resulting bam files were merged by replicate, and log2 (RPM-normalized ChIP) / (RPM-normalized Input) bigwig files were generated using Bedtools (bamcompare). We identified putative Pho motifs occurrence within the *hb* genomic region using PWMScan (PWMTools, ccg.epfl.ch) (Ambrosini et al., 2018) by selecting Pho_DROME_B1H OTF0277.1 (OnTheFly 2014 motif library) with a p-value cutoff at 5.10^{-4}.

Hb vs Pho target analysis

Putative Hb binding target genes were extracted from pan-neuroblast Hb DamID sequencing data (Sen et al., 2019). Dam-only and Hb-Dam raw reads were re-analyzed for peak detection using damidseq_pipeline (Marshall and Brand, 2015). The resulting list was further filtered to include only those with genome-wide *hb* PWM occurrences (PWMscan (Ambrosini et al., 2018) for HUNB_DROME_SELEX_OTF0231.1 from OnTheFly2014 library using $1e^{-4}$ p-value) resulting in 884 genes, annotated by PAVIS (Huang et al., 2013) (dm6.05, 5kb upstream and 1kb downstream), that contain Hb peaks overlapping with a *hb* binding motif. Chromatin accessible ("open") Pho motifs in stage 12 neuroblasts were extracted by intersecting the genome-wide Pho-PWM/ChIP list with Stage 12 ATAC-seq peak summit data, as described below: The Pho PWM/ChIP list contains genomic Pho motif occurrences (see *ChIP-seq analysis* section) that also have Pho ChIP peaks in L3 larval brain (Brown et al., 2018) or late stage embryo Pho ChIP peaks (Bonnet et al., 2019). Stage 12 ATAC-seq peak summit list was generated by running MACS2 (Zhang et al., 2008) on the ATAC Stage 12 neuroblast replicate-merged bam file (Huang et al., 2013) (callpeak with following option: -f BAMPE, -q 0.05, -slocal 10000, -nomodel, -shift -100, -extsize 200, -nolambda). To score for the presence of Pho-motifs within the chromatin accessible regions, each analyzed ATAC peak was restricted to a region that contained the summit and surrounding accessible sequences corresponding to 20% of the peak width. The resulting list was annotated to the closest gene using the PAVIS webtool (manticore.niehs.nih.gov/pavis2). Finally, the Hb putative target genes list and the Stage-12-Open-Pho-PWM/ChIP target genes list were compared (210 genes intersect) and the result was tested against a random model. The random model consists of randomly picking 210 non-Hb target 10'000 times and quantify their intersection with the Stage-12-Open-Pho-PWM/ChIP

target list. All data intersections were done using Bedtools (Quinlan and Hall, 2010) (intersect -wa).

Statistical analysis

We applied standard t-tests using Prism v8. Statistical significance was classified as followed: ** ≤ 0.01, *** ≤ 0.001, **** ≤ 0.0001. For competence window tests, N's represent each neuroblast lineage quantified by a minimum of three embryos per genotype. For DNA FISH tests, N's represent each embryo, and number of FISH signals quantified are shown on the graph. Graphs show each data point used for statistical analysis, and bars indicate mean and standard deviation. To estimate the P-value of bootstrap simulation we use the following formula*: pval = (1 + sum(s >= s0)) / (N+1)*, in which *s* is random values and *s0* is the observed value.

Supplemental information:

Table S1

Supplemental Figures S1-S7

References

Allan, D.W., and Thor, S. (2015). Transcriptional selectors, masters, and combinatorial codes: regulatory principles of neural subtype specification. Wiley Interdiscip Rev Dev Biol *4*, 505-528.

Ambrosini, G., Groux, R., and Bucher, P. (2018). PWMScan: a fast tool for scanning entire genomes with a position-specific weight matrix. Bioinformatics *34*, 2483-2484.

Awasaki, T., Kao, C.F., Lee, Y.J., Yang, C.P., Huang, Y., Pfeiffer, B.D., Luan, H., Jing, X., Huang, Y.F., He, Y., *et al.* (2014). Making Drosophila lineage-restricted drivers via patterned recombination in neuroblasts. Nat Neurosci *17*, 631-637.

Bantignies, F., Roure, V., Comet, I., Leblanc, B., Schuettengruber, B., Bonnet, J., Tixier, V., Mas, A., and Cavalli, G. (2011). Polycomb-dependent regulatory contacts between distant Hox loci in Drosophila. Cell *144*, 214-226.

Bentsen, M., Goymann, P., Schultheis, H., Klee, K., Petrova, A., Wiegandt, R., Fust, A., Preussner, J., Kuenne, C., Braun, T., *et al.* (2020). ATAC-seq footprinting unravels kinetics of transcription factor binding during zygotic genome activation. Nat Commun *11*, 4267.

Beuchle, D., Struhl, G., and Muller, J. (2001). Polycomb group proteins and heritable silencing of Drosophila Hox genes. Development *128*, 993-1004.

Bonev, B., Mendelson Cohen, N., Szabo, Q., Fritsch, L., Papadopoulos, G.L., Lubling, Y., Xu, X., Lv, X., Hugnot, J.P., Tanay, A., *et al.* (2017). Multiscale 3D Genome Rewiring during Mouse Neural Development. Cell *171*, 557-572 e524.

Bonnet, J., Lindeboom, R.G.H., Pokrovsky, D., Stricker, G., Celik, M.H., Rupp, R.A.W., Gagneur, J., Vermeulen, M., Imhof, A., and Muller, J. (2019). Quantification of Proteins and Histone Marks in Drosophila Embryos Reveals Stoichiometric Relationships Impacting Chromatin Regulation. Dev Cell *51*, 632-644 e636.

Boyle, S., Flyamer, I.M., Williamson, I., Sengupta, D., Bickmore, W.A., and Illingworth, R.S. (2020). A central role for canonical PRC1 in shaping the 3D nuclear landscape. Genes Dev *34*, 931-949.

Brand, A.H., and Perrimon, N. (1993). Targeted gene expression as a means of altering cell fates and generating dominant phenotypes. Development *118*, 401-415.

Brody, T., and Odenwald, W.F. (2000). Programmed transformations in neuroblast gene expression during Drosophila CNS lineage development. Dev Biol *226*, 34-44.

Bronshtein, I., Kanter, I., Kepten, E., Lindner, M., Berezin, S., Shav-Tal, Y., and Garini, Y. (2016). Exploring chromatin organization mechanisms through its dynamic properties. Nucleus *7*, 27-33.

Brown, J.L., Sun, M.A., and Kassis, J.A. (2018). Global changes of H3K27me3 domains and Polycomb group protein distribution in the absence of recruiters Spps or Pho. Proc Natl Acad Sci U S A *115*, E1839-E1848.

Buenrostro, J.D., Giresi, P.G., Zaba, L.C., Chang, H.Y., and Greenleaf, W.J. (2013). Transposition of native chromatin for fast and sensitive epigenomic profiling of open chromatin, DNA-binding proteins and nucleosome position. Nat Methods *10*, 1213-1218.

Buenrostro, J.D., Wu, B., Chang, H.Y., and Greenleaf, W.J. (2015). ATAC-seq: A Method for Assaying Chromatin Accessibility Genome-Wide. Curr Protoc Mol Biol *109*, 21 29 21-29.

Chan, L.N., and Gehring, W. (1971). Determination of blastoderm cells in Drosophila melanogaster. Proc Natl Acad Sci U S A *68*, 2217-2221.

Cheutin, T., and Cavalli, G. (2018). Loss of PRC1 induces higher-order opening of Hox loci independently of transcription during Drosophila embryogenesis. Nat Commun *9*, 3898.

Classen, A.K., Bunker, B.D., Harvey, K.F., Vaccari, T., and Bilder, D. (2009). A tumor suppressor activity of Drosophila Polycomb genes mediated by JAK-STAT signaling. Nat Genet *41*, 1150-1155.

Cleary, M.D., and Doe, C.Q. (2006). Regulation of neuroblast competence: multiple temporal identity factors specify distinct neuronal fates within a single early competence window. Genes Dev *20*, 429-434.

Cruz-Molina, S., Respuela, P., Tebartz, C., Kolovos, P., Nikolic, M., Fueyo, R., van Ijcken, W.F.J., Grosveld, F., Frommolt, P., Bazzi, H., *et al.* (2017). PRC2 Facilitates the Regulatory Topology Required for Poised Enhancer Function during Pluripotent Stem Cell Differentiation. Cell Stem Cell *20*, 689-705 e689.

Cusanovich, D.A., Reddington, J.P., Garfield, D.A., Daza, R.M., Aghamirzaie, D., Marco-Ferreres, R., Pliner, H.A., Christiansen, L., Qiu, X., Steemers, F.J., *et al.* (2018). The cis-regulatory dynamics of embryonic development at single-cell resolution. Nature *555*, 538-542.

Desai, A.R., and McConnell, S.K. (2000). Progressive restriction in fate potential by neural progenitors during cerebral cortical development. Development *127*, 2863-2872.

Doe, C.Q. (2017). Temporal Patterning in the Drosophila CNS. Annu Rev Cell Dev Biol *33*, 219-240.

Eagen, K.P., Aiden, E.L., and Kornberg, R.D. (2017). Polycomb-mediated chromatin loops revealed by a subkilobase-resolution chromatin interaction map. Proc Natl Acad Sci U S A *114*, 8764-8769.

Elliott, J., Jolicoeur, C., Ramamurthy, V., and Cayouette, M. (2008). Ikaros confers early temporal competence to mouse retinal progenitor cells. Neuron *60*, 26-39.

Finlan, L.E., Sproul, D., Thomson, I., Boyle, S., Kerr, E., Perry, P., Ylstra, B., Chubb, J.R., and Bickmore, W.A. (2008). Recruitment to the nuclear periphery can alter expression of genes in human cells. PLoS Genet *4*, e1000039.

Gentile, C., Berlivet, S., Mayran, A., Paquette, D., Guerard-Millet, F., Bajon, E., Dostie, J., and Kmita, M. (2019). PRC2-Associated Chromatin Contacts in the Developing Limb Reveal a Possible Mechanism for the Atypical Role of PRC2 in HoxA Gene Expression. Dev Cell.

Gozalo, A., Duke, A., Lan, Y., Pascual-Garcia, P., Talamas, J.A., Nguyen, S.C., Shah, P.P., Jain, R., Joyce, E.F., and Capelson, M. (2020). Core Components of the Nuclear Pore Bind Distinct States of Chromatin and Contribute to Polycomb Repression. Mol Cell *77*, 67-81 e67.

Grossniklaus, U., and Paro, R. (2014). Transcriptional silencing by polycomb-group proteins. Cold Spring Harb Perspect Biol *6*, a019331.

Guelen, L., Pagie, L., Brasset, E., Meuleman, W., Faza, M.B., Talhout, W., Eussen, B.H., de Klein, A., Wessels, L., de Laat, W., *et al.* (2008). Domain organization of human chromosomes revealed by mapping of nuclear lamina interactions. Nature *453*, 948-951.

Haines, J.E., and Eisen, M.B. (2018). Patterns of chromatin accessibility along the anterior-posterior axis in the early Drosophila embryo. PLoS Genet *14*, e1007367.

Harr, J.C., Luperchio, T.R., Wong, X., Cohen, E., Wheelan, S.J., and Reddy, K.L. (2015). Directed targeting of chromatin to the nuclear lamina is mediated by chromatin state and A-type lamins. J Cell Biol *208*, 33-52.

Harrison, D.A., Binari, R., Nahreini, T.S., Gilman, M., and Perrimon, N. (1995). Activation of a Drosophila Janus kinase (JAK) causes hematopoietic neoplasia and developmental defects. EMBO J *14*, 2857-2865.

Hesselberth, J.R., Chen, X., Zhang, Z., Sabo, P.J., Sandstrom, R., Reynolds, A.P., Thurman, R.E., Neph, S., Kuehn, M.S., Noble, W.S., *et al.* (2009). Global mapping of protein-DNA interactions in vivo by digital genomic footprinting. Nat Methods *6*, 283-289.

Hirabayashi, Y., Suzki, N., Tsuboi, M., Endo, T.A., Toyoda, T., Shinga, J., Koseki, H., Vidal, M., and Gotoh, Y. (2009). Polycomb limits the neurogenic competence of neural precursor cells to promote astrogenic fate transition. Neuron *63*, 600-613.

Hirono, K., Margolis, J.S., Posakony, J.W., and Doe, C.Q. (2012). Identification of hunchback cis-regulatory DNA conferring temporal expression in neuroblasts and neurons. Gene expression patterns : GEP *12*, 11-17.

Huang, W., Loganantharaj, R., Schroeder, B., Fargo, D., and Li, L. (2013). PAVIS: a tool for Peak Annotation and Visualization. Bioinformatics *29*, 3097-3099.

Isshiki, T., Pearson, B., Holbrook, S., and Doe, C.Q. (2001). Drosophila neuroblasts sequentially express transcription factors which specify the temporal identity of their neuronal progeny. Cell *106*, 511-521.

Jeong, J.Y., Yim, H.S., Ryu, J.Y., Lee, H.S., Lee, J.H., Seen, D.S., and Kang, S.G. (2012). One-step sequence- and ligation-independent cloning as a rapid and versatile cloning method for functional genomics studies. Appl Environ Microbiol *78*, 5440-5443.

Kanai, M.I., Okabe, M., and Hiromi, Y. (2005). seven-up Controls switching of transcription factors that specify temporal identities of Drosophila neuroblasts. Developmental cell *8*, 203-213.

Kent, W.J., Zweig, A.S., Barber, G., Hinrichs, A.S., and Karolchik, D. (2010). BigWig and BigBed: enabling browsing of large distributed datasets. Bioinformatics *26*, 2204-2207.

King, I.F., Emmons, R.B., Francis, N.J., Wild, B., Muller, J., Kingston, R.E., and Wu, C.T. (2005). Analysis of a polycomb group protein defines regions that link repressive activity on nucleosomal templates to in vivo function. Mol Cell Biol *25*, 6578-6591.

Kohwi, M., and Doe, C.Q. (2013). Temporal fate specification and neural progenitor competence during development. Nature reviews Neuroscience *14*, 823-838.

Kohwi, M., Lupton, J.R., Lai, S.L., Miller, M.R., and Doe, C.Q. (2013). Developmentally regulated subnuclear genome reorganization restricts neural progenitor competence in Drosophila. Cell *152*, 97-108.

Kundu, S., Ji, F., Sunwoo, H., Jain, G., Lee, J.T., Sadreyev, R.I., Dekker, J., and Kingston, R.E. (2017). Polycomb Repressive Complex 1 Generates Discrete Compacted Domains that Change during Differentiation. Mol Cell *65*, 432-446 e435.

Langmead, B., and Salzberg, S.L. (2012). Fast gapped-read alignment with Bowtie 2. Nat Methods *9*, 357-359.

Li, H., Handsaker, B., Wysoker, A., Fennell, T., Ruan, J., Homer, N., Marth, G., Abecasis, G., and Durbin, R. (2009). The Sequence Alignment/Map format and SAMtools. Bioinformatics *25*, 2078-2079.

Lucas, T., and Kohwi, M. (2019). From insects to mammals: regulation of genome architecture in neural development. Curr Opin Neurobiol *59*, 146-156.

Marshall, O.J., and Brand, A.H. (2015). damidseq_pipeline: an automated pipeline for processing DamID sequencing datasets. Bioinformatics *31*, 3371-3373.

Martin, M. (2011). Cutadapt removes adapter sequences from high-throughput sequencing reads. 2011 *17*, 3.

Mattar, P., Ericson, J., Blackshaw, S., and Cayouette, M. (2015). A conserved regulatory logic controls temporal identity in mouse neural progenitors. Neuron *85*, 497-504.

McKay, D.J., and Lieb, J.D. (2013). A common set of DNA regulatory elements shapes Drosophila appendages. Dev Cell *27*, 306-318.

Meister, P., Towbin, B.D., Pike, B.L., Ponti, A., and Gasser, S.M. (2010). The spatial dynamics of tissue-specific promoters during C. elegans development. Genes Dev *24*, 766-782.

Meng, J.L., Marshall, Z.D., Lobb-Rabe, M., and Heckscher, E.S. (2019). How prolonged expression of Hunchback, a temporal transcription factor, re-wires locomotor circuits. Elife *8*.

Milon, B., Sun, Y., Chang, W., Creasy, T., Mahurkar, A., Shetty, A., Nurminsky, D., and Nurminskaya, M. (2014). Map of open and closed chromatin domains in Drosophila genome. BMC Genomics *15*, 988.

Miyares, R.L., and Lee, T. (2019). Temporal control of Drosophila central nervous system development. Curr Opin Neurobiol *56*, 24-32.

Negre, N., Hennetin, J., Sun, L.V., Lavrov, S., Bellis, M., White, K.P., and Cavalli, G. (2006). Chromosomal distribution of PcG proteins during Drosophila development. PLoS biology *4*, e170.

Oktaba, K., Gutierrez, L., Gagneur, J., Girardot, C., Sengupta, A.K., Furlong, E.E., and Muller, J. (2008). Dynamic regulation by polycomb group protein complexes controls pattern formation and the cell cycle in Drosophila. Dev Cell *15*, 877-889.

Papp, B., and Muller, J. (2006). Histone trimethylation and the maintenance of transcriptional ON and OFF states by trxG and PcG proteins. Genes Dev *20*, 2041-2054.

Patel, T., Tursun, B., Rahe, D.P., and Hobert, O. (2012). Removal of Polycomb repressive complex 2 makes C. elegans germ cells susceptible to direct conversion into specific somatic cell types. Cell Rep *2*, 1178-1186.

Pearson, B.J., and Doe, C.Q. (2003). Regulation of neuroblast competence in Drosophila. Nature *425*, 624-628.

Peric-Hupkes, D., Meuleman, W., Pagie, L., Bruggeman, S.W., Solovei, I., Brugman, W., Graf, S., Flicek, P., Kerkhoven, R.M., van Lohuizen, M., *et al.* (2010). Molecular maps of the reorganization of genome-nuclear lamina interactions during differentiation. Mol Cell *38*, 603-613.

Peric-Hupkes, D., and van Steensel, B. (2010). Role of the nuclear lamina in genome organization and gene expression. Cold Spring Harb Symp Quant Biol *75*, 517-524.

Pickersgill, H., Kalverda, B., de Wit, E., Talhout, W., Fornerod, M., and van Steensel, B. (2006). Characterization of the Drosophila melanogaster genome at the nuclear lamina. Nature genetics *38*, 1005-1014.

Qin, P., Parlak, M., Kuscu, C., Bandaria, J., Mir, M., Szlachta, K., Singh, R., Darzacq, X., Yildiz, A., and Adli, M. (2017). Live cell imaging of low- and non-repetitive chromosome loci using CRISPR-Cas9. Nat Commun *8*, 14725.

898 Quinlan, A.R., and Hall, I.M. (2010). BEDTools: a flexible suite of utilities for comparing
899 genomic features. Bioinformatics *26*, 841-842.

900 Ramirez, F., Ryan, D.P., Gruning, B., Bhardwaj, V., Kilpert, F., Richter, A.S., Heyne, S.,
901 Dundar, F., and Manke, T. (2016). deepTools2: a next generation web server for deep-
902 sequencing data analysis. Nucleic Acids Res *44*, W160-165.

903 Reddy, K.L., Zullo, J.M., Bertolino, E., and Singh, H. (2008). Transcriptional repression
904 mediated by repositioning of genes to the nuclear lamina. Nature *452*, 243-247.

905 Ross-Innes, C.S., Stark, R., Teschendorff, A.E., Holmes, K.A., Ali, H.R., Dunning, M.J., Brown,
906 G.D., Gojis, O., Ellis, I.O., Green, A.R., *et al.* (2012). Differential oestrogen receptor binding is
907 associated with clinical outcome in breast cancer. Nature *481*, 389-393.

908 Rossi, A.M., Fernandes, V.M., and Desplan, C. (2017). Timing temporal transitions during brain
909 development. Curr Opin Neurobiol *42*, 84-92.

910 Rothwell, W.F.a.S., W. (2000). Fluorescent analysis of Drosophila embryos (Cold Spring
911 Harbor: Cold Spring Harbor Press).

912 Saad, H., Gallardo, F., Dalvai, M., Tanguy-le-Gac, N., Lane, D., and Bystricky, K. (2014). DNA
913 dynamics during early double-strand break processing revealed by non-intrusive imaging of
914 living cells. PLoS Genet *10*, e1004187.

915 Schindelin, J., Arganda-Carreras, I., Frise, E., Kaynig, V., Longair, M., Pietzsch, T., Preibisch,
916 S., Rueden, C., Saalfeld, S., Schmid, B., *et al.* (2012). Fiji: an open-source platform for
917 biological-image analysis. Nat Methods *9*, 676-682.

918 Schuettengruber, B., and Cavalli, G. (2009). Recruitment of polycomb group complexes and
919 their role in the dynamic regulation of cell fate choice. Development *136*, 3531-3542.

920 Schwartz, Y.B., Kahn, T.G., Nix, D.A., Li, X.Y., Bourgon, R., Biggin, M., and Pirrotta, V.
921 (2006). Genome-wide analysis of Polycomb targets in Drosophila melanogaster. Nat Genet *38*,
922 700-705.

923 Sen, S.Q., Chanchani, S., Southall, T.D., and Doe, C.Q. (2019). Neuroblast-specific open
924 chromatin allows the temporal transcription factor, Hunchback, to bind neuroblast-specific loci.
925 Elife *8*.

926 Seroka, A.Q., and Doe, C.Q. (2019). The Hunchback temporal transcription factor determines
927 motor neuron axon and dendrite targeting in Drosophila. Development *146*.

928 Shevelyov, Y.Y., and Nurminsky, D.I. (2011). The Nuclear Lamina as a Gene-silencing Hub.
929 Current issues in molecular biology *14*, 27-38.

930 Struhl, G. (1981). A gene product required for correct initiation of segmental determination in
931 Drosophila. Nature *293*, 36-41.

Telley, L., Agirman, G., Prados, J., Amberg, N., Fievre, S., Oberst, P., Bartolini, G., Vitali, I., Cadilhac, C., Hippenmeyer, S., *et al.* (2019). Temporal patterning of apical progenitors and their daughter neurons in the developing neocortex. Science *364*.

Tie, F., Furuyama, T., and Harte, P.J. (1998). The Drosophila Polycomb Group proteins ESC and E(Z) bind directly to each other and co-localize at multiple chromosomal sites. Development *125*, 3483-3496.

Tolhuis, B., Blom, M., Kerkhoven, R.M., Pagie, L., Teunissen, H., Nieuwland, M., Simonis, M., de Laat, W., van Lohuizen, M., and van Steensel, B. (2011). Interactions among Polycomb domains are guided by chromosome architecture. PLoS genetics *7*, e1001343.

Tolhuis, B., de Wit, E., Muijrers, I., Teunissen, H., Talhout, W., van Steensel, B., and van Lohuizen, M. (2006). Genome-wide profiling of PRC1 and PRC2 Polycomb chromatin binding in Drosophila melanogaster. Nat Genet *38*, 694-699.

Touma, J.J., Weckerle, F.F., and Cleary, M.D. (2012). Drosophila Polycomb complexes restrict neuroblast competence to generate motoneurons. Development *139*, 657-666.

Van Bortle, K., and Corces, V.G. (2013). Spinning the web of cell fate. Cell *152*, 1213-1217.

van Steensel, B., and Belmont, A.S. (2017). Lamina-Associated Domains: Links with Chromosome Architecture, Heterochromatin, and Gene Repression. Cell *169*, 780-791.

Venken, K.J., Carlson, J.W., Schulze, K.L., Pan, H., He, Y., Spokony, R., Wan, K.H., Koriabine, M., de Jong, P.J., White, K.P., *et al.* (2009). Versatile P[acman] BAC libraries for transgenesis studies in Drosophila melanogaster. Nat Methods *6*, 431-434.

Williams, R.R., Azuara, V., Perry, P., Sauer, S., Dvorkina, M., Jorgensen, H., Roix, J., McQueen, P., Misteli, T., Merkenschlager, M., *et al.* (2006). Neural induction promotes large-scale chromatin reorganisation of the Mash1 locus. J Cell Sci *119*, 132-140.

Wimmer, E.A., Carleton, A., Harjes, P., Turner, T., and Desplan, C. (2000). Bicoid-independent formation of thoracic segments in Drosophila. Science *287*, 2476-2479.

Zhang, Y., Liu, T., Meyer, C.A., Eeckhoute, J., Johnson, D.S., Bernstein, B.E., Nusbaum, C., Myers, R.M., Brown, M., Li, W., *et al.* (2008). Model-based analysis of ChIP-Seq (MACS). Genome Biol *9*, R137.

Zullo, J.M., Demarco, I.A., Pique-Regi, R., Gaffney, D.J., Epstein, C.B., Spooner, C.J., Luperchio, T.R., Bernstein, B.E., Pritchard, J.K., Reddy, K.L., *et al.* (2012). DNA sequence-dependent compartmentalization and silencing of chromatin at the nuclear lamina. Cell *149*, 1474-1487.

KEY RESOURCES TABLE

REAGENT or RESOURCE	SOURCE	IDENTIFIER
Antibodies		
Chicken polyclonal anti-HA	Bethyl Laboratories	Cat#A190-106A; RRID:AB_66692
Chicken polyclonal anti-GFP	Aves Labs	Cat#GFP-1010; RRID:AB_2307313
Rat monoclonal anti-HA (3F10)	Sigma-Aldrich	Cat#11867423001; RRID:AB_390918
Rat monoclonal anti-Deadpan (11D1CH11)	Abcam	Cat#ab195172
Rat monoclonal anti-Worniu (5A3AD2)	Abcam	Cat#ab196362
Rabbit polyclonal anti-Hunchback	Kind gift from Dr. Chris Doe, University of Oregon	N/A
Mouse monoclonal anti-Eve (3C10)	Developmental Studies Hybridoma Bank (DSHB)	Cat#3C10-c; RRID:AB_528229
Mouse monoclonal anti-Elav (9F8A9)	DSHB	Cat#9F8A9-s; RRID:AB_2314364
Rabbit polyclonal anti-Lamin R-836	Kind gift from Dr. Paul Fischer, Stony Brook University	N/A
Mouse monoclonal anti-Psc (6E8)	DSHB	Cat#6E8-s; RRID:AB_528437
Rabbit polyclonal anti-E(z)	Kind gift from Dr. Jürg Müller, Max-Planck Institute of Biochemistry	N/A
Mouse monoclonal anti-Abd-B (1A2E9)	DSHB	Cat#1A2E9; RRID:AB_528061
Rabbit polyclonal anti-H3K27me3	Sigma-Aldrich	Cat#07-449; RRID: AB_310624

Mouse anti-mNeonGreen	Antibodies-online	Cat#ABIN5608502
Rabbit polyclonal anti-Histone H3	Abcam	Cat#ab5176; RRID:AB_304763
Bacterial and Virus Strains		
SW102 E. coli containing 32kb-HA-hb BAC	Kohwi et al. 2013	N/A
TransforMax™ EPI300™ Electrocompetent E. coli	Lucigen	EC300110
Biological Samples		
Chemicals, Peptides, and Recombinant Proteins		
Halocarbon oil 27	Sigma-Aldrich	H8773; Cas: 9002-83-9
Fetal Bovine Serum	Sigma-Aldrich	12306C
Calcein Violet 450AM Viability Dye	Thermo Fisher Scientific	65-0854-39
7-AAD Viability Staining Solution	Thermo Fisher Scientific	00-6993-50
SYBR® Green I Nucleic Acid Gel Stain	Thermo Fisher Scientific	S7563
DAPI	Thermo Fisher Scientific	D3571
AMPure XP beads	Beckman Coulter	A63880
TDE1 (Tagment DNA Enzyme, Tn5)	Illumina	15027865
NEBNext High-Fidelity 2x PCR MM	NEB	m0541s
Normal Goat Serum	Jackson ImmunoResearch	005-000-121
Aqua-Poly/Mount	Polysciences	18606

Chan and Gehring's Balanced Saline (C&G Medium)	Chan et al., 1971	N/A
Fisherbrand Sterile Cell Strainers (40µm)	Fisher Scientific	22363547
Bel-Art™ SP Scienceware™ Flowmi™ Cell Strainers (40µm)	Fisher Scientific	14100150
DWK Life Sciences Wheaton™ Dounce Tissue Grinders	Fisher Scientific	357542
Critical Commercial Assays		
NextSeq 500/550 High Output Kit v2.5 (75 Cycles)	Illumina	20024906
PhiX CONTROL V3 KIT	Illumina	FC-110-3001
High Sensitivity DNA Kit	Agilent	5067-4626
Qubit™ dsDNA HS Assay Kit	Thermo Fisher Scientific	Q32851
DNA Clean & Concentrator-5	Zymo Research	D4013
FISH Tag™ DNA Orange Kit, with Alexa Fluor™ 555 dye	Thermo Fisher Scientific	F32948
HiSpeed Plasmid Midi Kit	Qiagen	12643
Deposited Data		
Stages 5, 10, and 12_sortedNB_ATACseq	This study	NCBI SRA accession number PRJNA754600
Experimental Models: Cell Lines		
Experimental Models: Organisms/Strains		
D. melanogaster: Psc^{h27} : Psc[h27]/CyO	Bloomington Drosophila Stock Center (BDSC)	Cat#5547; RRID:BDSC_5547

D. melanogaster: Psc[e24]: y[1] w[*]; P{ry[+t7.2]=neoFRT}42D Psc[e24]/SM6b, P{ry[+t7.2]=eve-lacZ8.0}SB1	BDSC	Cat#24155; RRID:BDSC_24155
D. melanogaster: E(z)[731]: w[*]; E(z)[731] P{1xFRT.G}2A/TM6C, Sb[1] Tb[1]	BDSC	Cat#24470; RRID:BDSC_24470
D. melanogaster: inscutable-gal4: w[*];P{w[+mW.hs]=GawB}insc [Mz1407]	BDSC	Cat#8751; RRID:BDSC_8751
D. melanogaster:CQ2-GAL4: y[1] w[*]; P{w[+mC]=CQ2-GAL4}O	BDSC	Cat#7466; RRID:BDSC_7466
D. melanogaster: en-GAL4: w[1118]; P{y[+t7.7] w[+mC]=GMR60F10-GAL4}attP2	BDSC	Cat#46438; RRID:BDSC_46438
D. melanogaster: UAS-hb	Wimmer et al., 2000	N/A
D. melanogaster: Psc-Su(z)2[P3C]	Classen et al., 2009	N/A
D. melanogaster: esc[6]/CyO	Struhl, 1981	N/A
D. melanogaster: esc[5]/CyO	Struhl, 1981	N/A
D. melanogaster: $Hb^{HA:WT}$	Kohwi et al., 2013	N/A
D. melanogaster: Dpn-eGFP	This paper	N/A
D. melanogaster: Hb[HA:Δintron]	This paper	N/A
D. melanogaster: w[1118]	BDSC	Cat#3605; RRID:BDSC_3605
Oligonucleotides		
Primers for the Hb DNA FISH probe, see Suppl.Table S1	Kohwi et al., 2013	N/A

Recombinant DNA		
NLS pEGFP-N3(1299)	Addgene	Cat#62043; RRID:Addgene_62043
Dpn-Gal80	Kind gift from Dr. Chris Doe, University of Oregon	N/A
Dpn-NLSpEGFP-N3	This paper	N/A
Hb[HA:WT] BAC	Kohwi et al., (2013)	N/A
Hb[HA:Δintron] BAC	This paper	N/A
PL-452 N-EGFP	AddGene	Cat#19173; RRID:Addgene_19173
Software and Algorithms		
bcl2fastq conversion software	Illumina	N/A
FASTQC	S. Andrews	http://www.bioinformatics.babraham.ac.uk/projects/fastqc/
Cutadapt	Martin et al., 2011	https://cutadapt.readthedocs.io/en/stable/
bowtie2	Langmead and Salzberg, 2012	https://github.com/BenLangmead/bowtie2
Picard Toolkit	Broad Institute	http://broadinstitute.github.io/picard
samtools	Li et al., 2009	http://www.htslib.org
BEDTools	Quinlan and Hall, 2010	https://github.com/arq5x/bedtools2
BedGraphToBigWig	Kent et al., 2010	http://hgdownload.cse.ucsc.edu/admin/exe/linux.x86_64/bedGraphToBigWig
MACS2	Zhang et al., 2008	https://github.com/macs3-project/MACS
deepTools2	Ramirez et al., 2016	https://github.com/deeptools/deepTools

DiffBind	Ross-Innes et al., 2012	https://bioconductor.org/packages/release/bioc/html/DiffBind.html
Fiji	Schindelin et al., 2012	https://fiji.sc

Figure 1

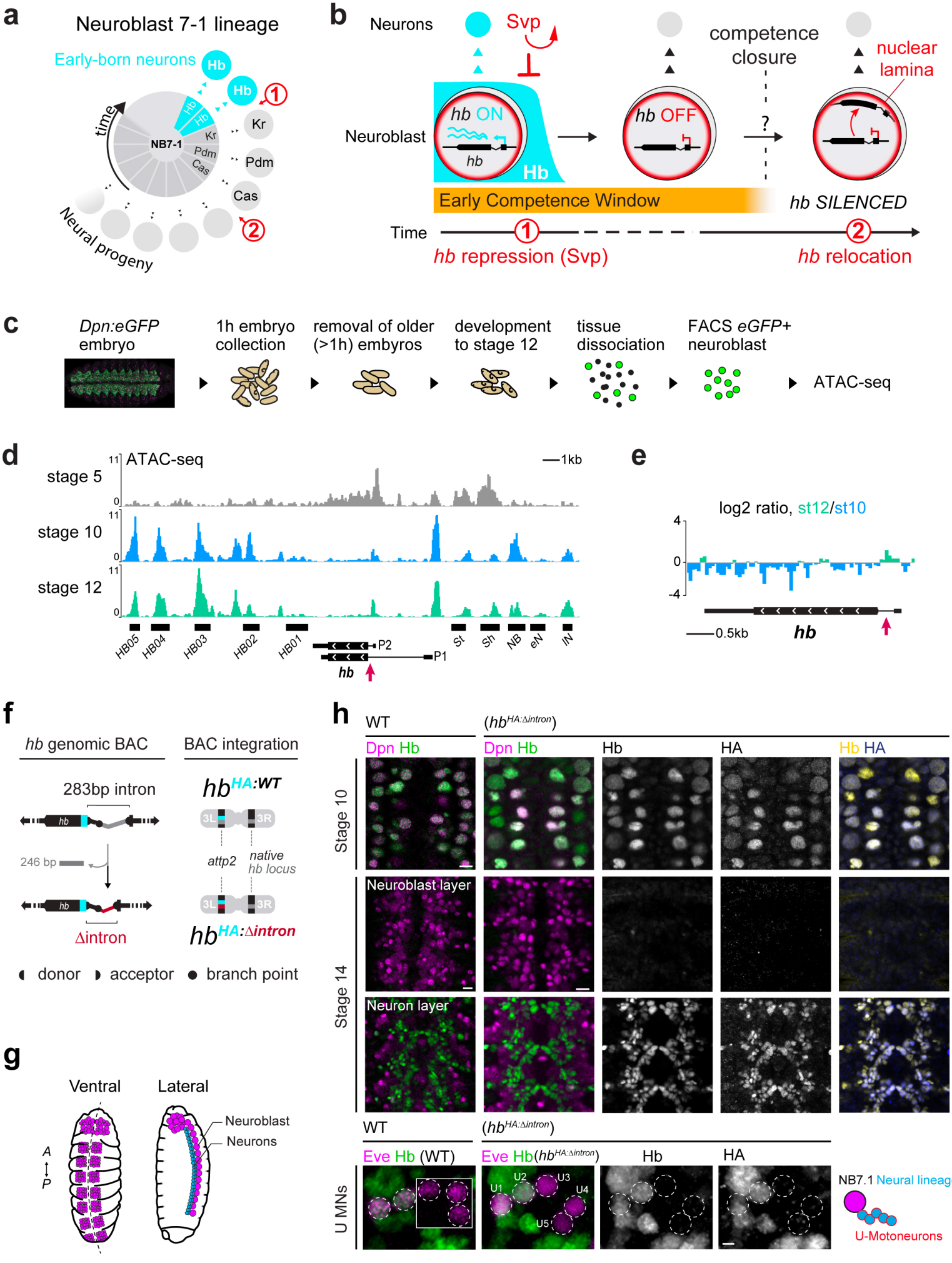

a
Neuroblast 7-1 lineage
Early-born neurons
Hb
Hb
Kr
Pdm
Cas
NB7-1
time
Neural progeny
b
Neurons
Svp
Neuroblast
hb ON
hb
Hb
hb OFF
competence closure
nuclear lamina
Early Competence Window
hb SILENCED
Time
hb repression (Svp)
hb relocation
c
Dpn:eGFP embryo
1h embryo collection
removal of older (>1h) embyros
development to stage 12
tissue dissociation
FACS eGFP+ neuroblast
ATAC-seq
d
ATAC-seq
1kb
stage 5
stage 10
stage 12
HB05
HB04
HB03
HB02
HB01
P2
P1
hb
St
Sh
NB
eN
iN
e
log2 ratio, st12/st10
0.5kb
hb
f
hb genomic BAC
BAC integration
283bp intron
246 bp
Δintron
hb^HA:WT
attp2
native hb locus
hb^HA:Δintron
donor
acceptor
branch point
g
Ventral
Lateral
A
P
Neuroblast
Neurons
h
WT
(hb^HA:Δintron)
Dpn Hb
Hb
HA
Hb HA
Stage 10
Stage 14
Neuroblast layer
Neuron layer
Eve Hb (WT)
U MNs
U1
U2
U3
U4
U5
NB7.1 Neural lineage
U-Motoneurons

Figure 2

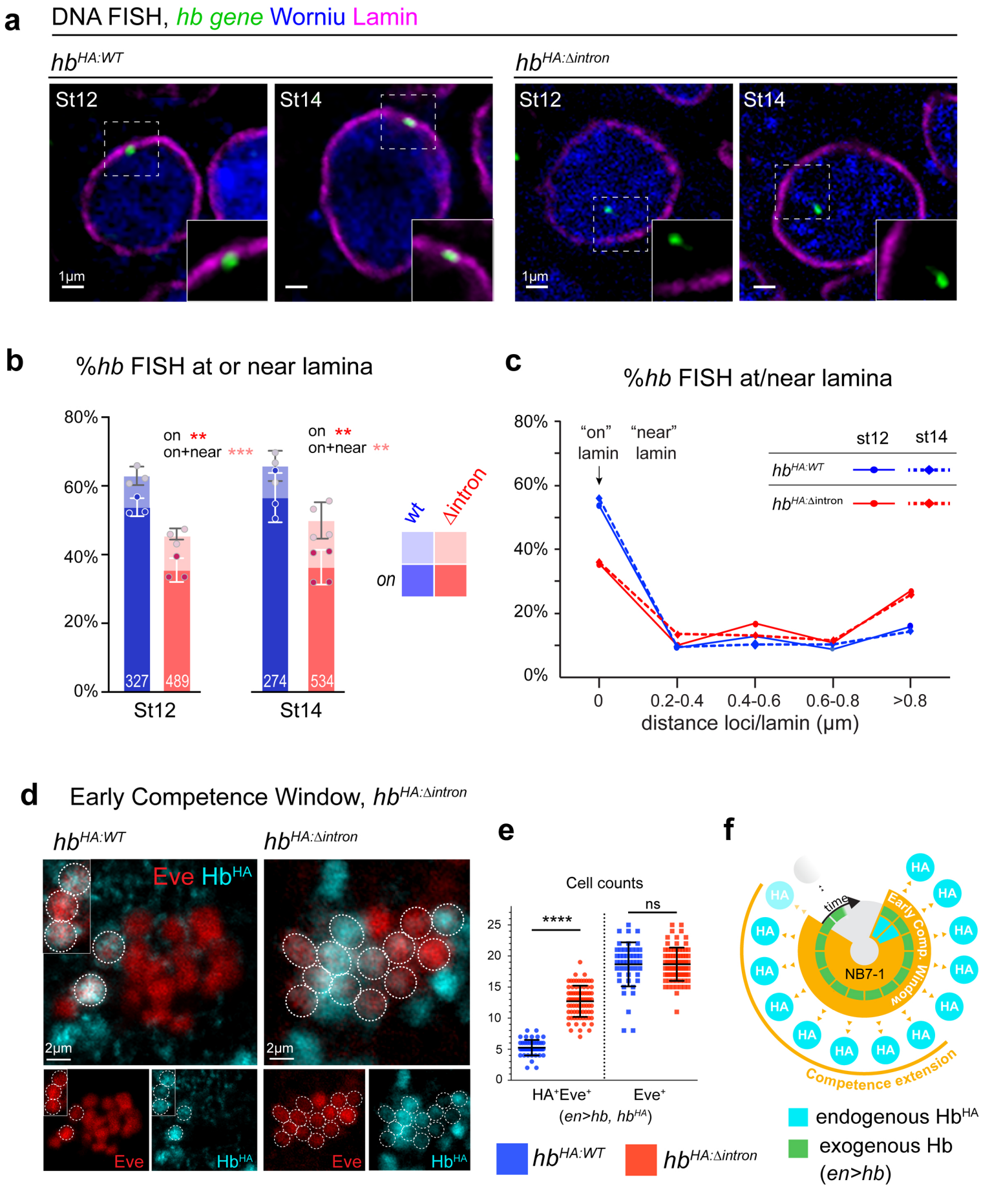

a
DNA FISH, hb gene Worniu Lamin
hbHA:WT
hbHA:Δintron
St12
St14
1µm
b
%hb FISH at or near lamina
80%
60%
40%
20%
0%
on **
on+near ***
on **
on+near **
327
489
274
534
St12
St14
wt
Δintron
on
c
%hb FISH at/near lamina
"on" lamin
"near" lamin
st12
st14
hbHA:WT
hbHA:Δintron
0
0.2-0.4
0.4-0.6
0.6-0.8
>0.8
distance loci/lamin (µm)
d
Early Competence Window, hbHA:Δintron
Eve HbHA
2µm
Eve
HbHA
e
Cell counts
****
ns
HA+Eve+
Eve+
(en>hb, hbHA)
hbHA:WT
hbHA:Δintron
f
HA
time
Early Comp. Window
NB7-1
Competence extension
endogenous HbHA
exogenous Hb
(en>hb)

Figure 3

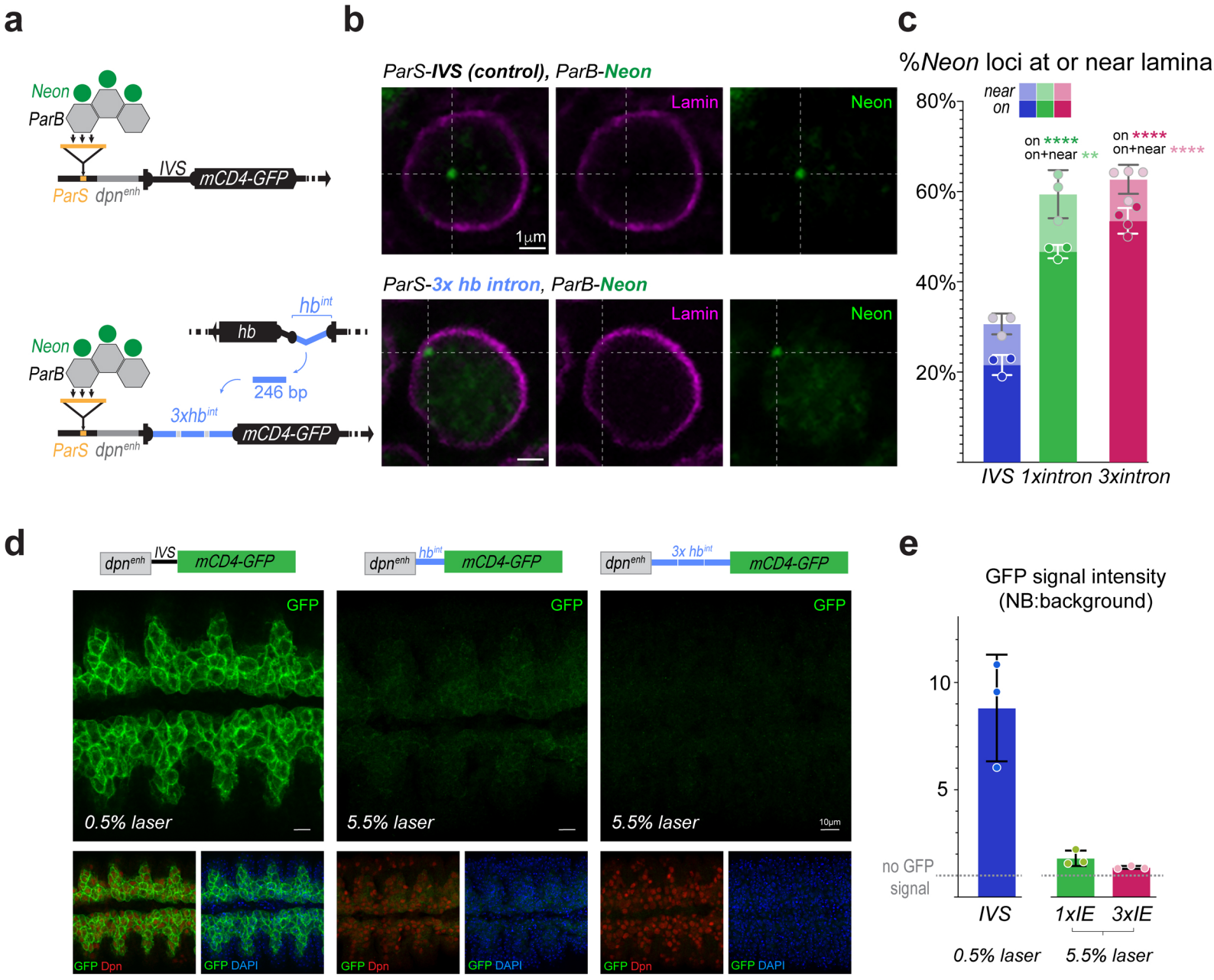

a
Neon
ParB
IVS
mCD4-GFP
ParS dpn^enh
hb^int
hb
246 bp
3xhb^int
b
ParS-IVS (control), ParB-Neon
Lamin
Neon
1µm
ParS-3x hb intron, ParB-Neon
c
%Neon loci at or near lamina
near
on
80%
60%
40%
20%
on ****
on+near **
on ****
on+near ****
IVS 1xintron 3xintron
d
dpn^enh
IVS
mCD4-GFP
hb^int
3x hb^int
GFP
0.5% laser
5.5% laser
10µm
GFP Dpn
GFP DAPI
e
GFP signal intensity
(NB:background)
10
5
no GFP signal
IVS
1xIE
3xIE
0.5% laser
5.5% laser

Figure 4

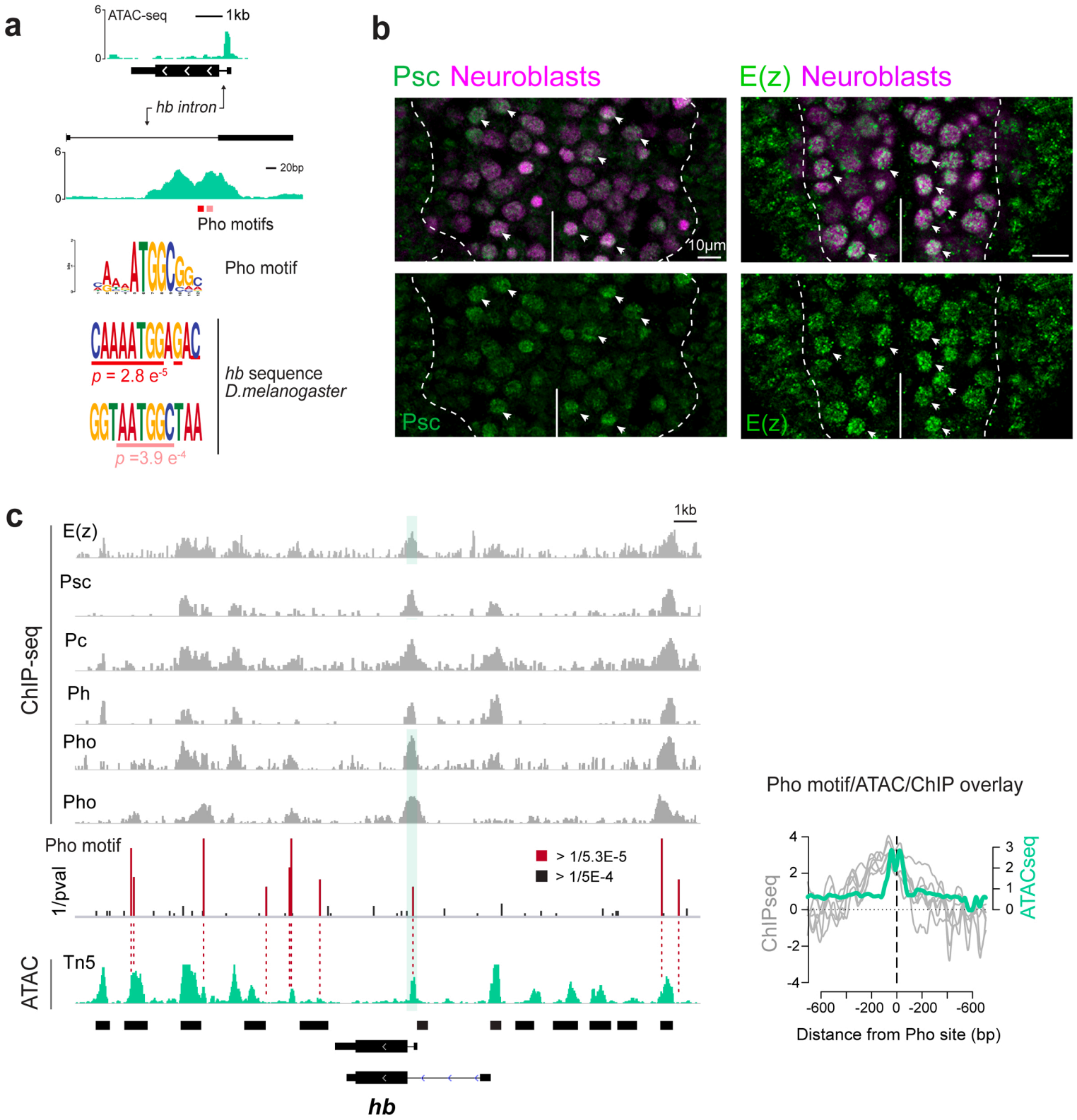

a
ATAC-seq
1kb
hb intron
20bp
Pho motifs
Pho motif
CAAAATGGAGAC
p = 2.8 e-5
GGTAATGGCTAA
p =3.9 e-4
hb sequence
D.melanogaster
b
Psc Neuroblasts
E(z) Neuroblasts
10µm
Psc
E(z)
c
1kb
E(z)
Psc
Pc
Ph
Pho
Pho
ChIP-seq
Pho motif
1/pval
> 1/5.3E-5
> 1/5E-4
ATAC
Tn5
hb
Pho motif/ATAC/ChIP overlay
ChIPseq
ATACseq
Distance from Pho site (bp)

Figure 5

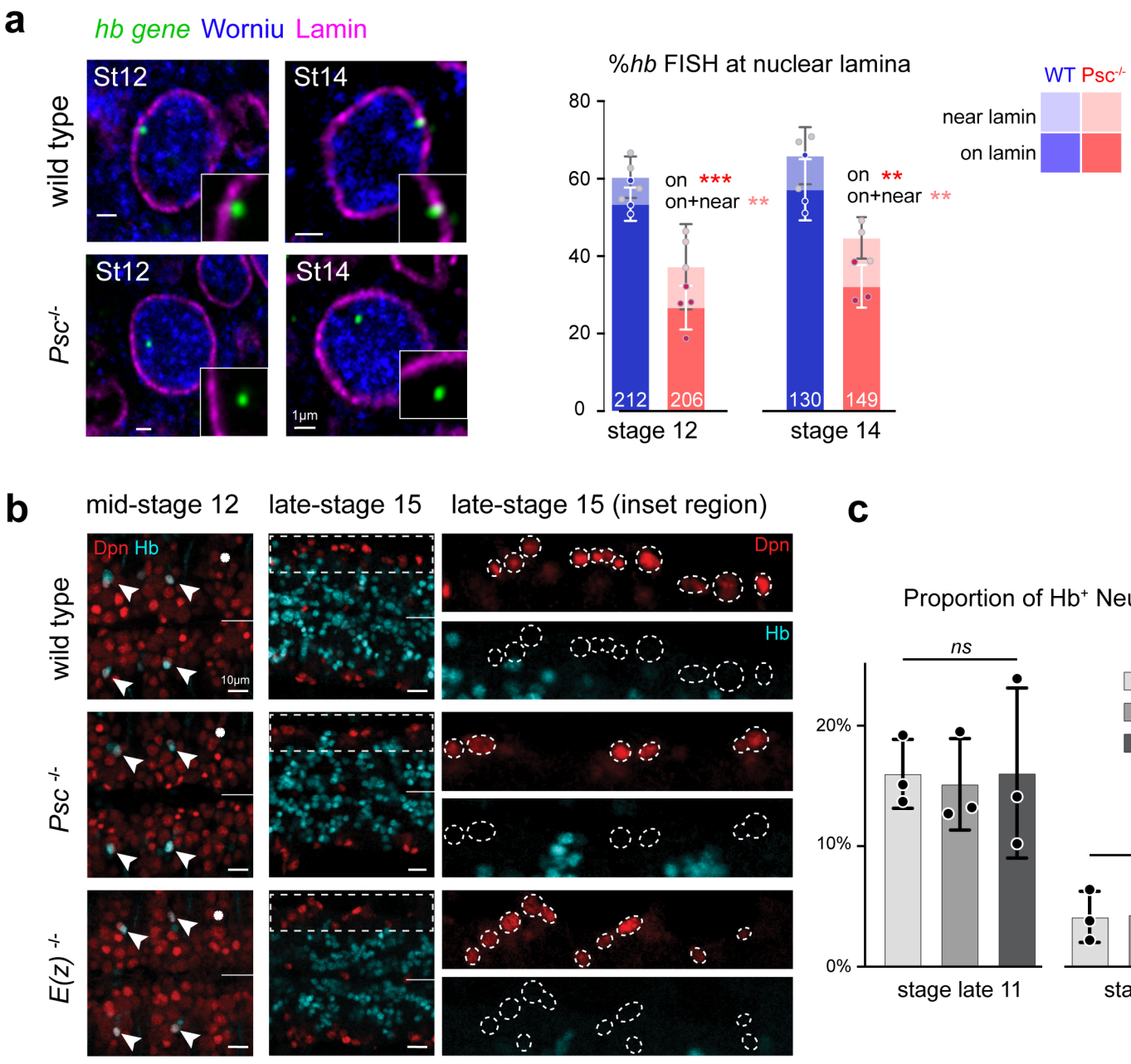

a
hb gene Worniu Lamin
wild type
Psc-/-
St12
St14
1µm
%hb FISH at nuclear lamina
WT Psc-/-
near lamin
on lamin
80
60
40
20
0
on ***
on+near **
on **
on+near **
212
206
130
149
stage 12
stage 14
b
mid-stage 12
late-stage 15
late-stage 15 (inset region)
Dpn Hb
Dpn
Hb
10µm
wild type
Psc -/-
E(z) -/-
c
Proportion of Hb+ Neuroblasts
ns
ns
20%
10%
0%
wild-type
Psc-/-
E(z)-/-
stage late 11
stage 12

Figure 6

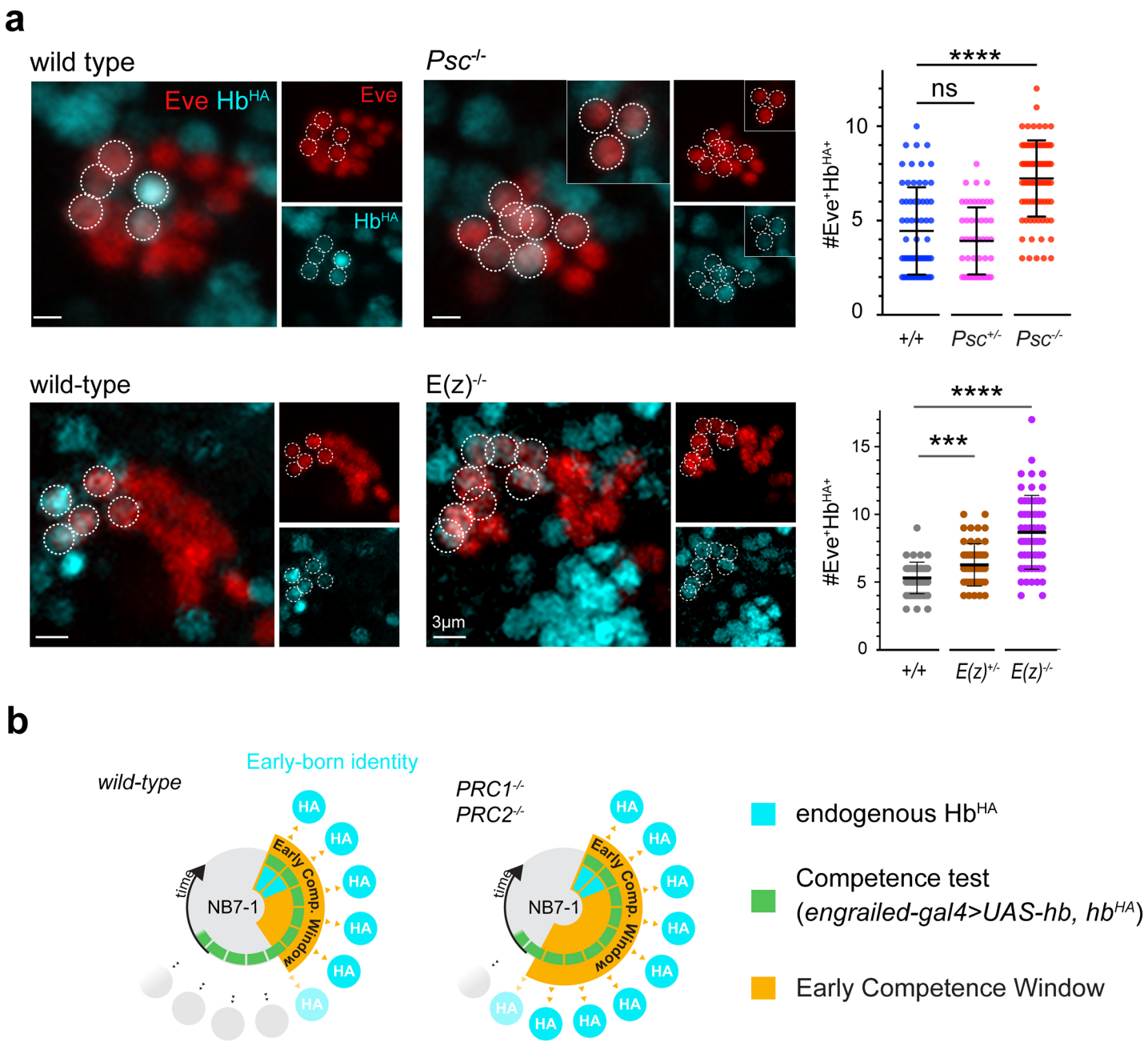
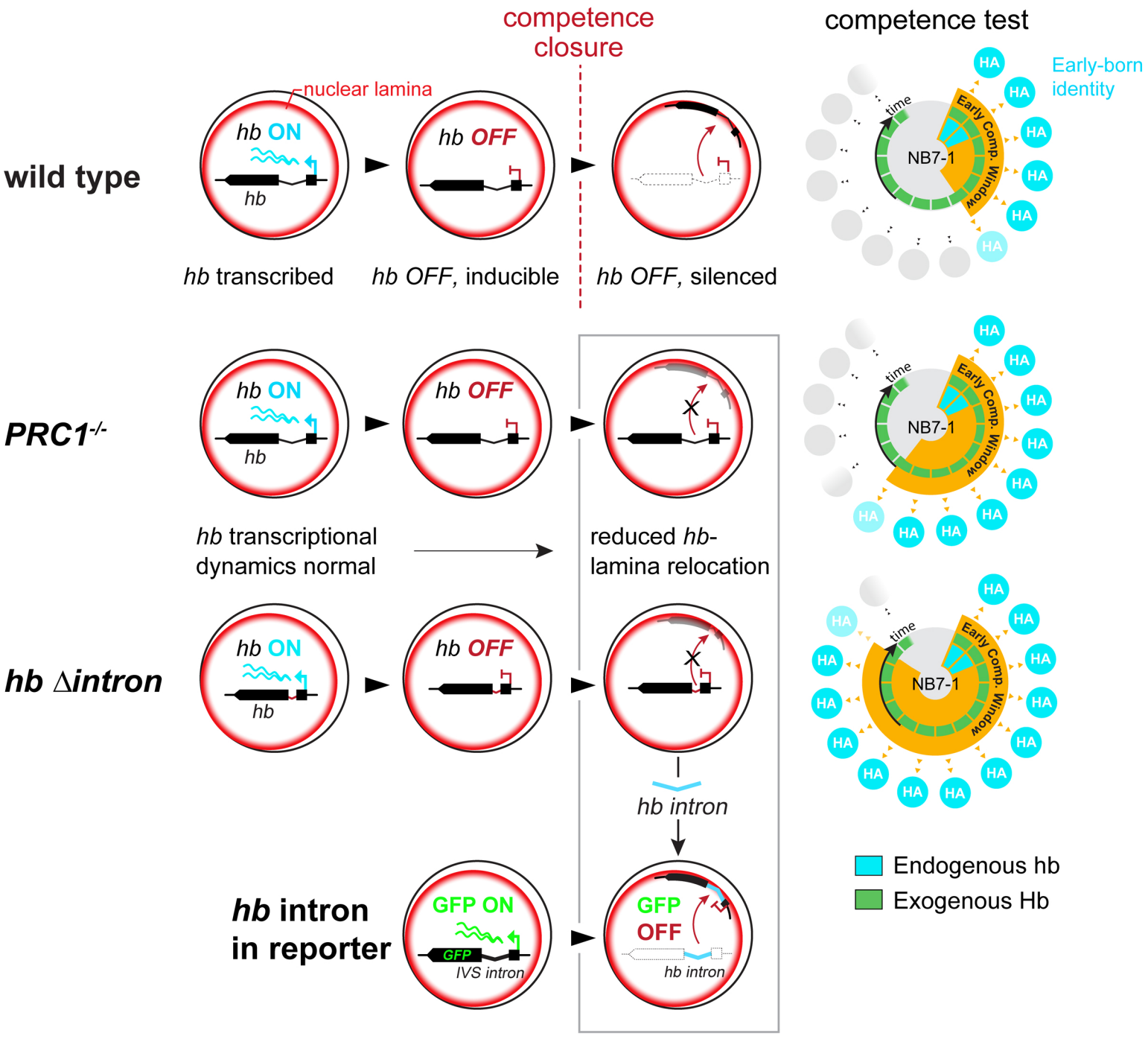

a
wild type
Eve Hb^HA
Eve
Hb^HA
Psc-/-
****
ns
#Eve+Hb^HA+
10
5
0
+/+
Psc+/-
Psc-/-
wild-type
E(z)-/-
3µm
****
***
15
10
5
0
+/+
E(z)+/-
E(z)-/-
b
wild-type
Early-born identity
PRC1-/-
PRC2-/-
time
NB7-1
Early Comp. Window
HA
endogenous Hb^HA
Competence test
(engrailed-gal4>UAS-hb, hb^HA)
Early Competence Window

Figure 7


competence closure
competence test
wild type
nuclear lamina
hb ON
hb
hb OFF
hb transcribed
hb OFF, inducible
hb OFF, silenced
Early-born identity
time
Early Comp. Window
NB7-1
HA
PRC1-/-
hb transcriptional dynamics normal
reduced hb-lamina relocation
hb Δintron
hb intron
hb intron in reporter
GFP ON
GFP
IVS intron
GFP OFF
Endogenous hb
Exogenous Hb

Supplemental information

Discrete cis-acting element regulates developmentally timed gene-lamina relocation and neural progenitor competence *in vivo*

T. Lucas, T.L. Hafer, H. Zhang, N. Molotkova and M. Kohwi

Correspondence to: mk3632@columbia.edu

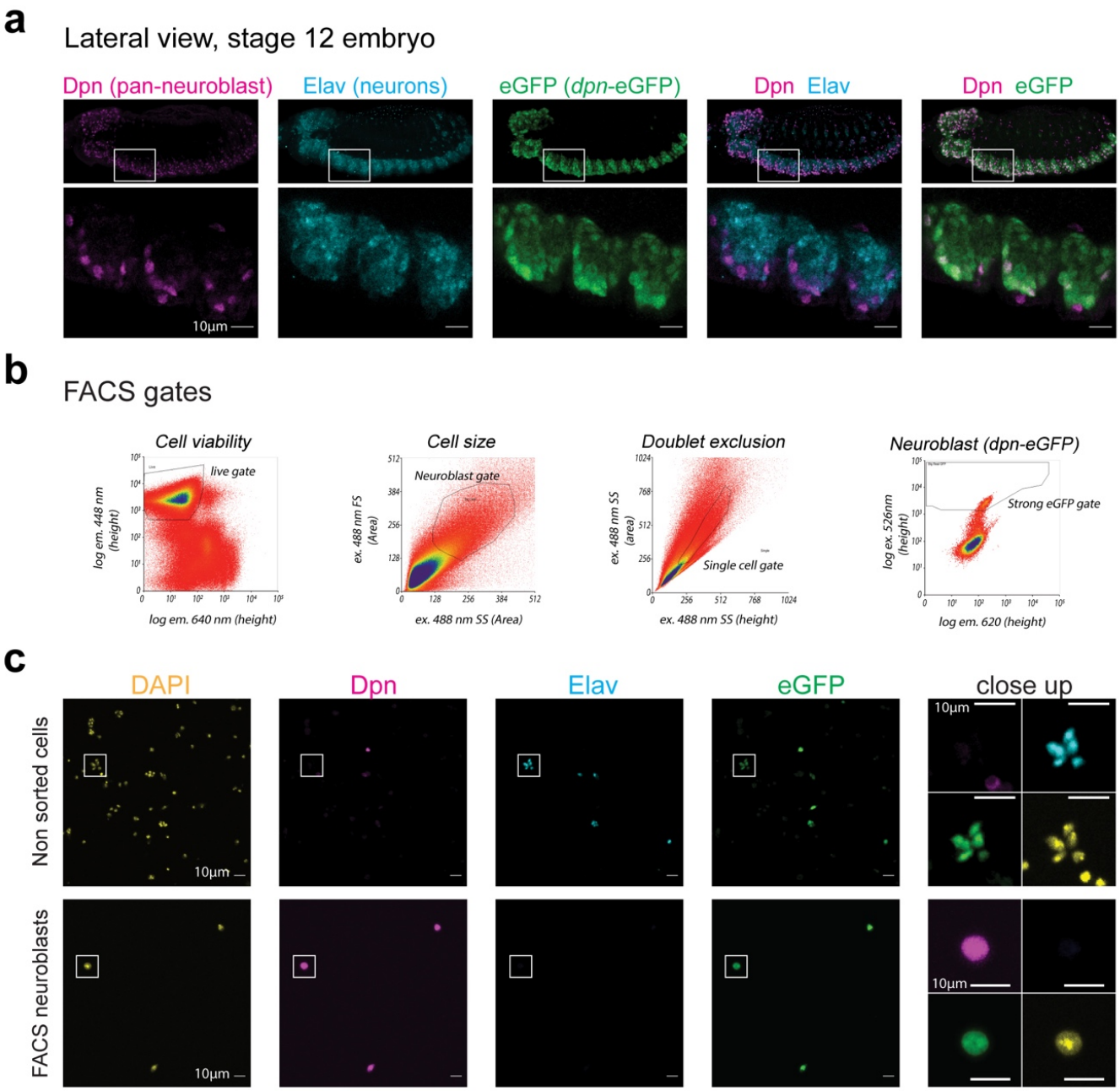
This PDF file includes:

Table S1

Supplemental S1-S7

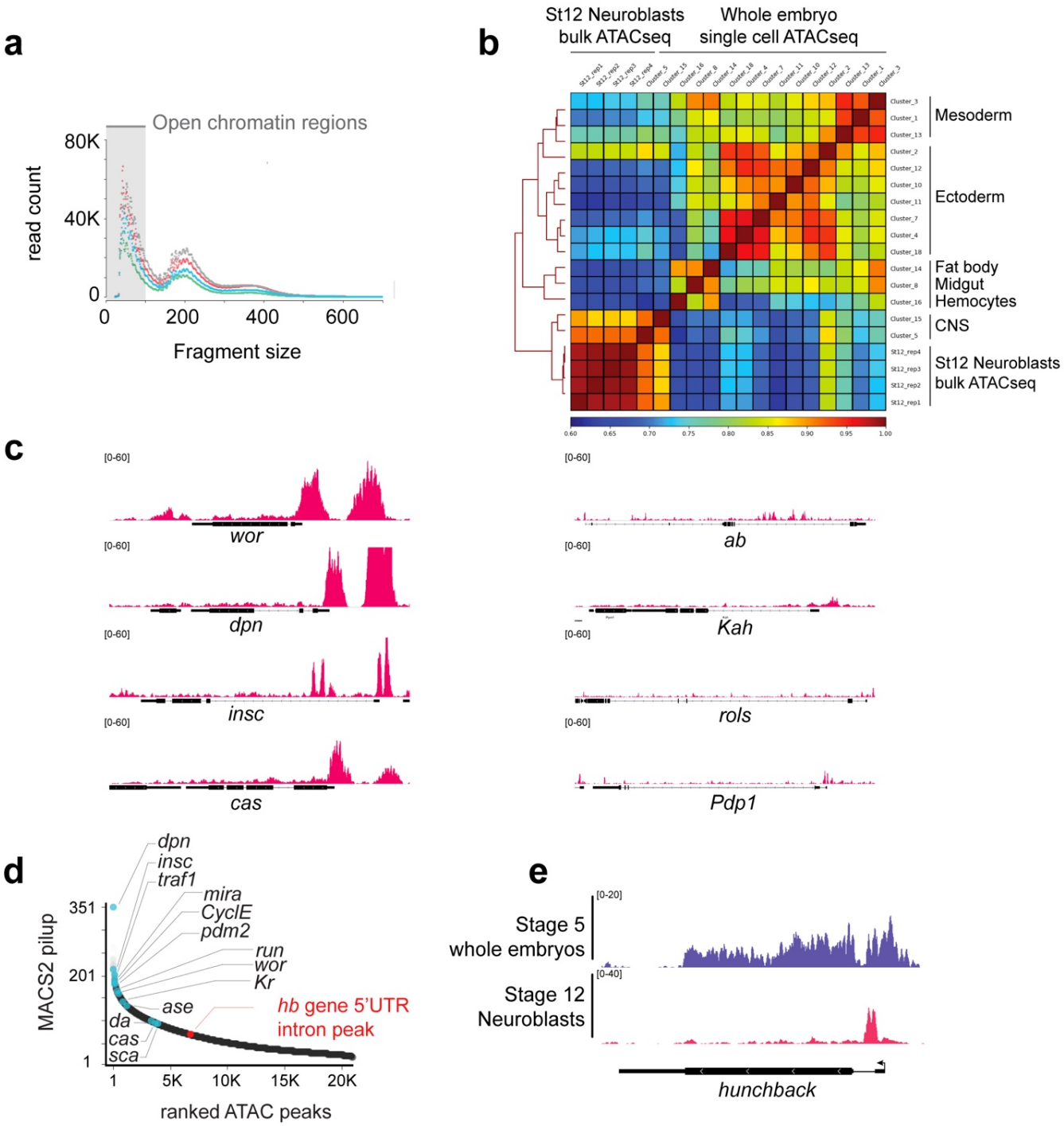
Table S1. Primers used to generate *hb* DNA FISH probe. Related to Figures 2 and 5.

Forward primer	Reverse primer
GAGGCTGCCGCTTGATTAACAC	ATCCAAGCAGGATCTCAGTAGC
AGGCTACTGAGATCCTGCTTGG	GCGTGGTTTGCTGTGGGAAATG
AAACGTGCCCTCCTGTTAAGTG	TAGATGGGCGGATATGGGTCTC
TCGAGTTCATCCCTCAACCTCC	GACAACAATTCCACTCAGCCAC
TGGCTGAGTGGAATTGTTGTCG	TCCTCCTTTCCCAGCTATTGAC
AGTCAATAGCTGGGAAAGGAGG	AGATGTGAGCCCAGTGTAATCC
GGGCAACTTTAAGCCCAGACAC	GGCATGGACTTTCGGCAATTAG
TCCAACATTACGCAGTACGCAG	CACTATTGTTTGGCCGCATAGC



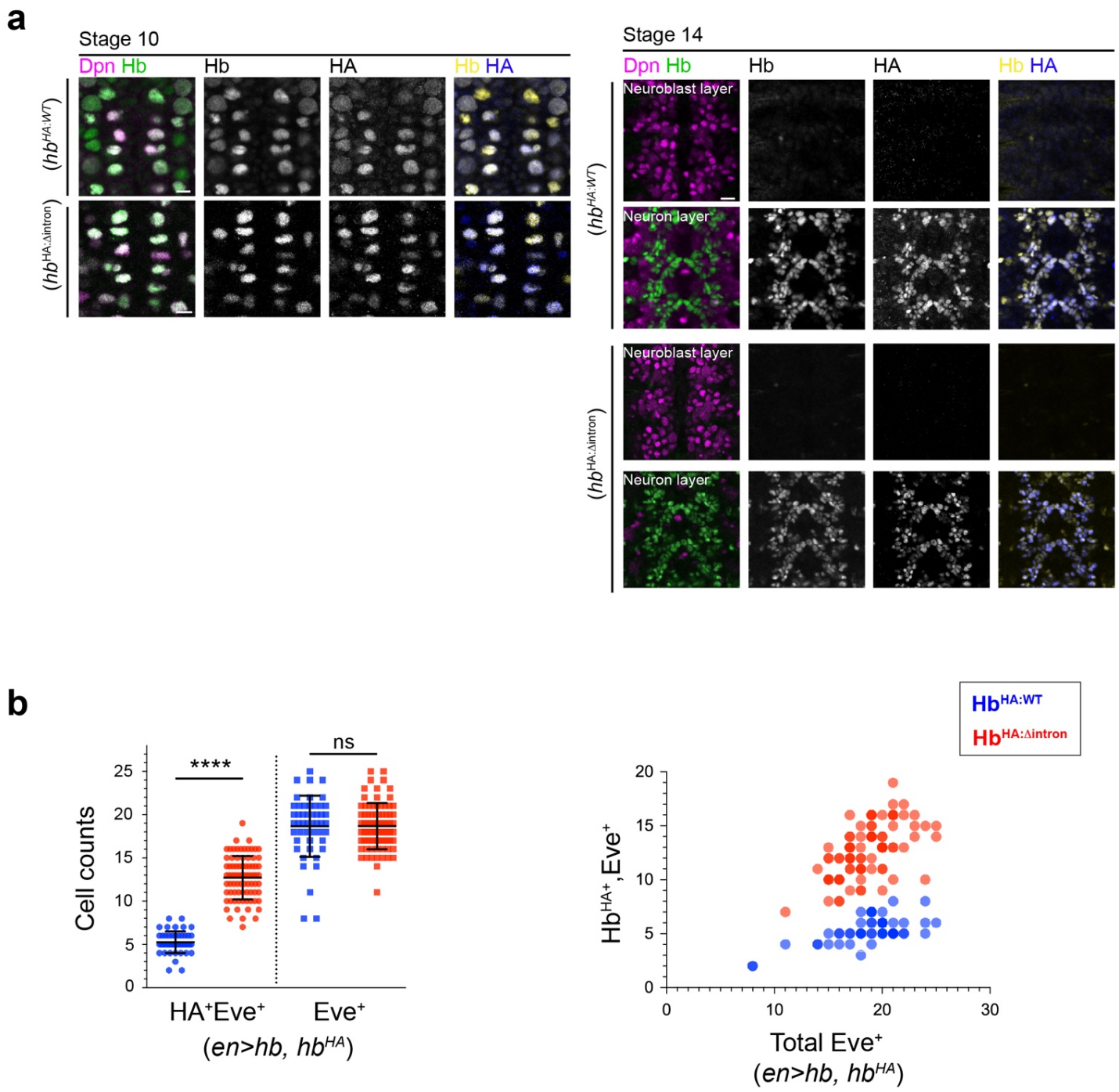
Supplemental Figure 1 (related to Figure 1). Neuroblast reporter and FACS validation.

a, Lateral views of stage 12 *dpn*-eGFP embryos immunostained for neuroblast marker, Dpn, neuronal marker, Elav, and GFP. Bottom panels show high magnification of inset. GFP is strong in neuroblasts but can be detected at lower levels in the neural progeny due to GFP perdurance. **b,** FACS scatter plots showing gates used to purify neuroblasts. Cell viability based on Calcein violet (viable) and 7AAD (dead) stains. **c,** Representative images of non-sorted cells (*top*) and sorted neuroblasts (*bottom*) stained with GFP, Dpn, and Elav. *Right*: high magnification of insets.

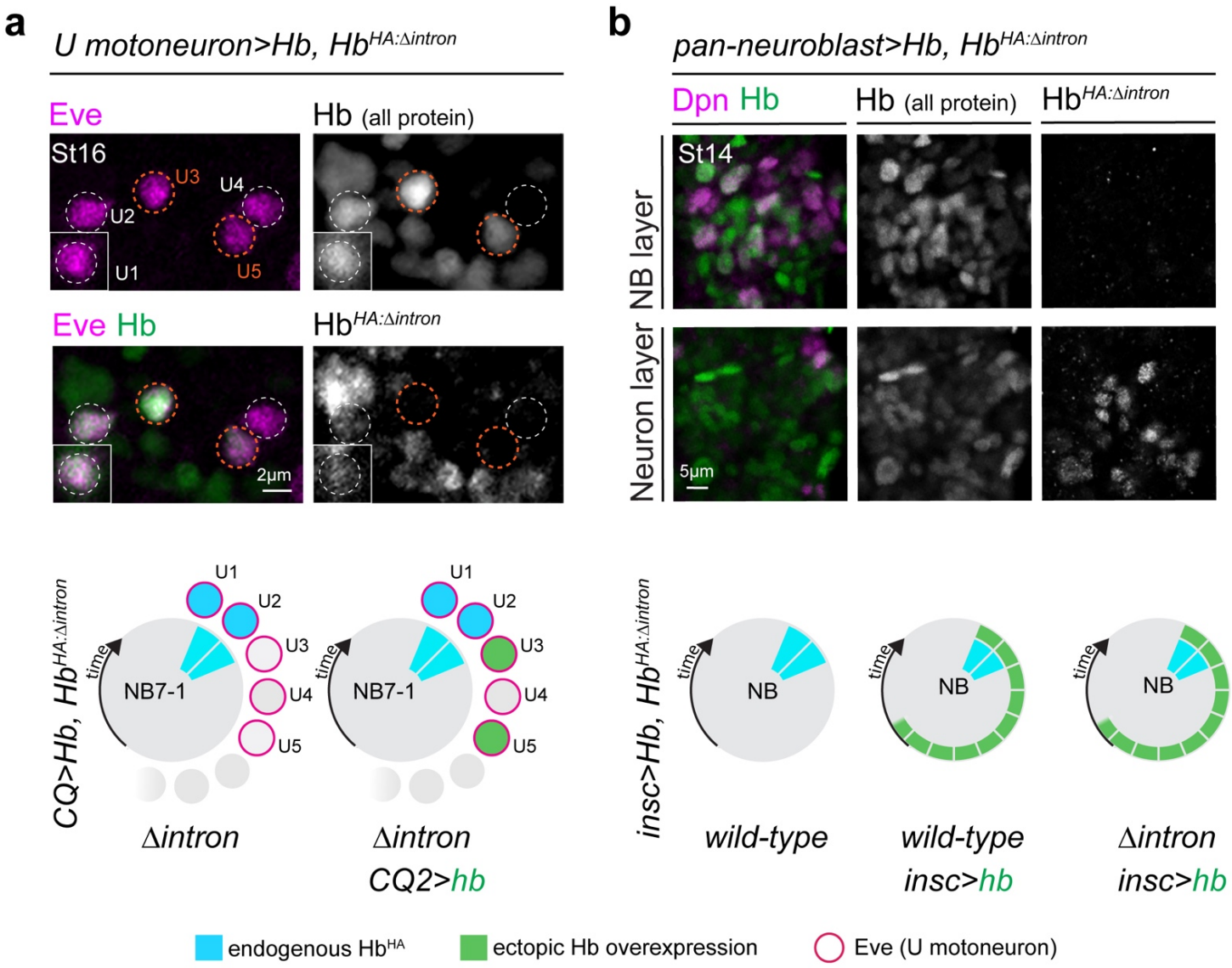


Supplemental Figure 2 (related to Figure 1): Validation of neuroblast-specific ATAC-seq data.

a, Distribution of fragment length from ATAC-seq libraries from four biological replicates of stage 12 FACS sorted neuroblasts. Open region peak (0-100bp), mono- nucleosome peak (150-250bp) and di-nucleosome peak (350-450bp) are visible. **b,** Pearson correlation heat map between stage 12 neuroblast ATAC-seq replicates (this paper) and all clusters from single cell ATAC- seq of whole, mid-embryogenic embryos (Cusanovich et al., 2018). **c,** ATAC-seq profile of example neuroblast genes (left) and non-neuroblast genes (right). **d,** ATAC peaks displayed ranked by amplitude (read pileup). A subset of neural genes expressed at stage 12 mid-embryogenesis is indicated along the distribution. **e,** reads per million normalized ATAC-seq profile spanning the *hb* locus at the cellular blastoderm Stage 5 (2-3h after egg laying, AEL) and the mid-embryogenesis Stage 12 (7-9h AEL). The *hb* locus is located on chromosome 3R.

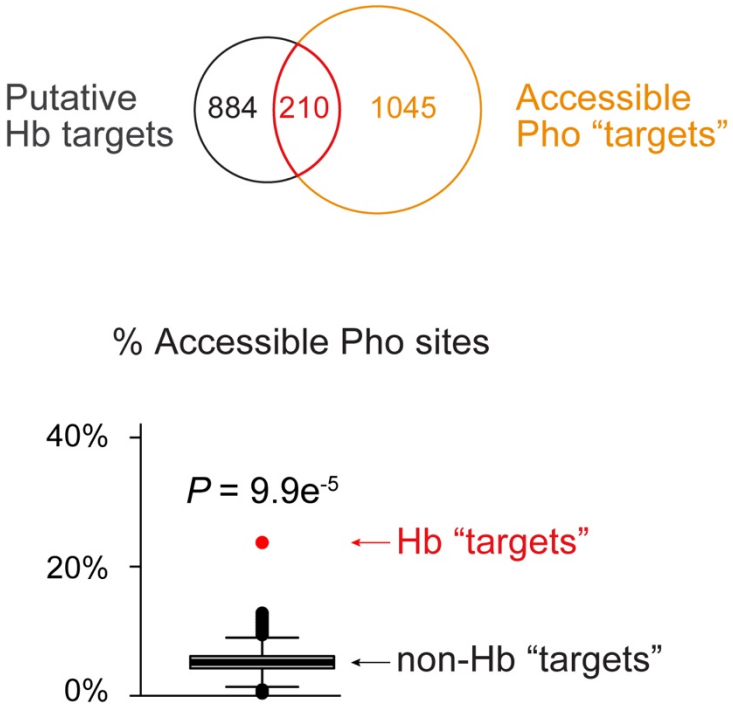


Supplemental Figure 3 (related to Figures 1 and 2): a, ventral nerve cord views of stage 10 and stage 14 $Hb^{HA:WT}$ and $Hb^{HA:\Delta intron}$ embryos immunostained with neuroblast marker, Dpn, Hb (all Hb protein), and HA (epitope for Hb protein derived only from BAC transgene). **b,** Quantified length of the early competence window for genotypes shown in a. *Left*: average length of early competence window (HA^+Eve^+) and total Eve cell number (Eve^+) in $Hb^{HA:WT}$ (blue) versus $Hb^{HA:\Delta intron}$ (red) genetic backgrounds. Data are represented as mean ± SD. *Right*: Corresponding scatter plots showing the number of Hb^{HA+} neurons relative to the number of Eve^+ cells in each NB7-1 lineage analyzed.



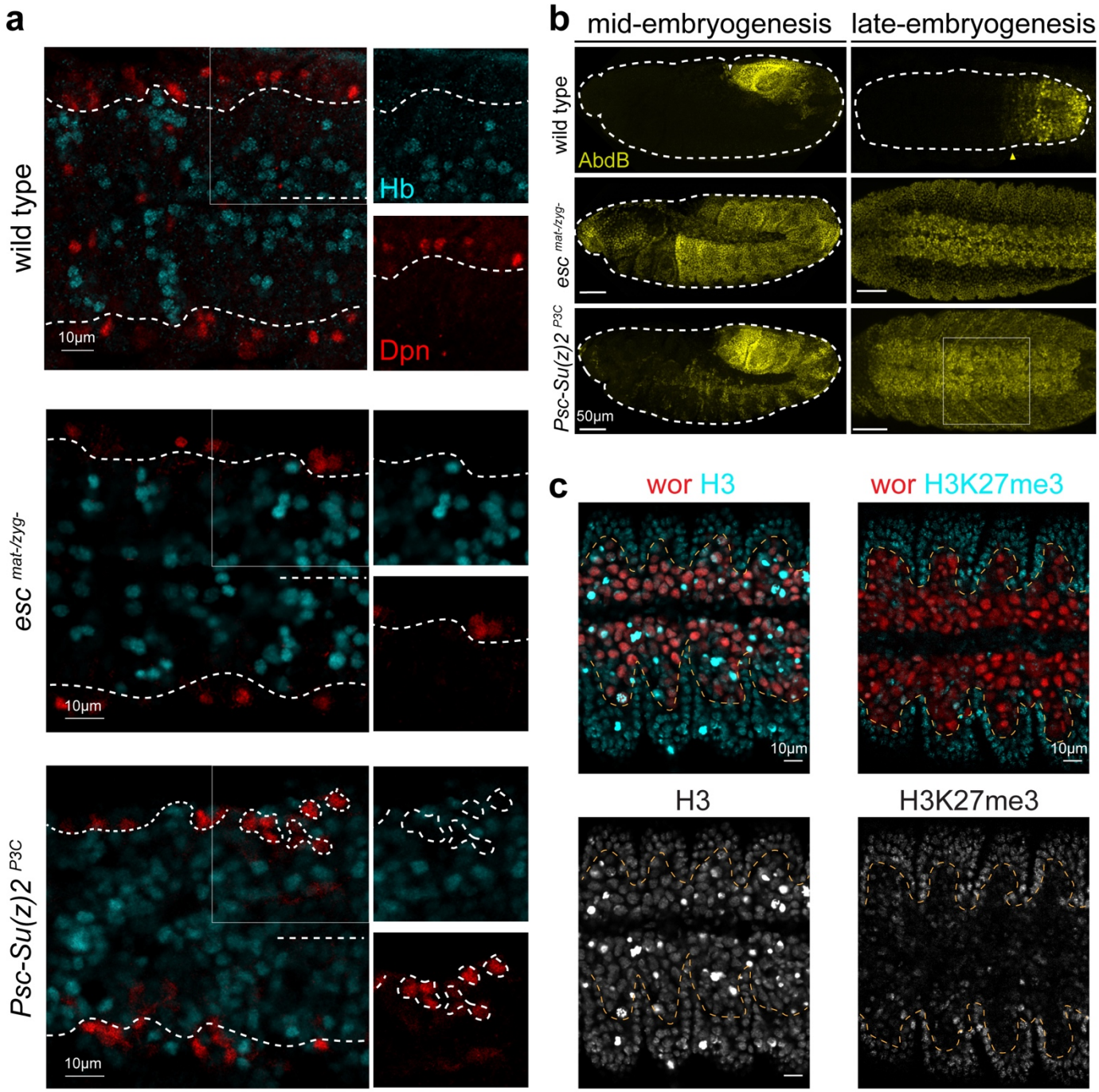
Supplemental Figure 4 (related to Figure 2): Exogenous Hb cannot induce $Hb^{HA:\Delta intron}$ directly within postmitotic neurons or within neuroblasts.

a, Stage 16 embryos stochastically misexpressing exogenous Hb (*cq2-gal4*, *UAShb*) in U-motoneurons (Eve^{+}) in the $Hb^{HA:\Delta intron}$ genetic background, immunostained for Eve, Hb and HA. Hb staining identifies late-born neurons (U3-U5) misexpressing Hb ectopically (see U3 and U5, orange dotted circles), HA staining identifies endogenous-Hb expression. **b,** Stage 14 embryos overexpressing Hb in all neuroblasts (*insc-gal4*, *UAShb*) in the $Hb^{HA:\Delta intron}$ background, immunostained for Dpn, Hb and HA. The neuroblast layer (top) and neuron layer (bottom) from a single hemisegment is shown. Schematic summaries are shown below each panel.



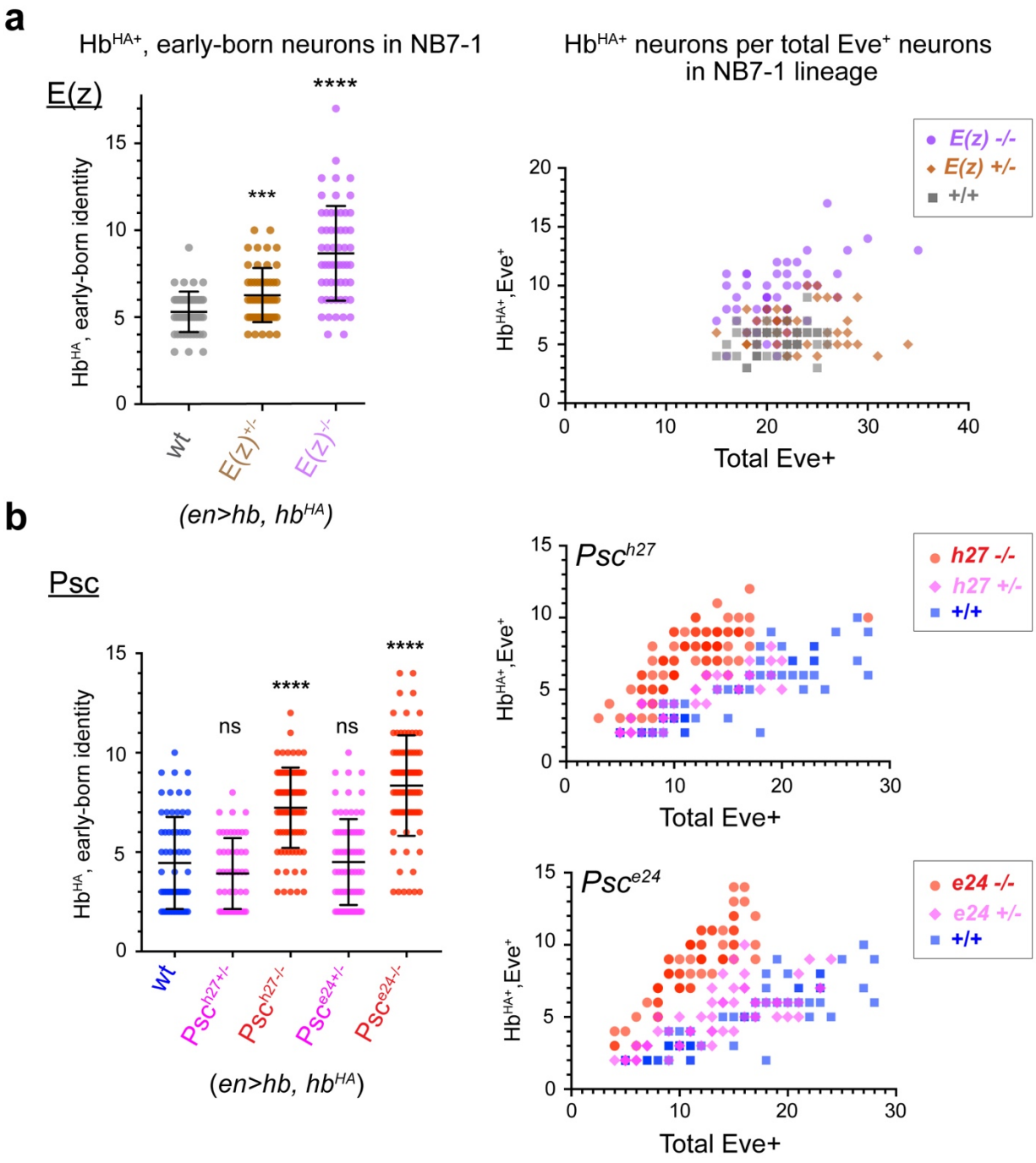
Supplemental Figure 5 (related to Figure 4).

Putative Hb targets which are genes in close proximity to Hb binding loci in the embryonic CNS (Sen et al., 2019) are found to be enriched for chromatin accessible Pho binding motifs in stage 12 neuroblasts compared to non-Hb targeted loci.



Supplemental Figure 6 (supplement to Figure 5): *hb* is not derepressed in strong PcG mutant alleles.

a, Ventral view of the VNC stained with Hb and neuroblast marker, Dpn in WT, maternal and zygotic *esc* mutant, and Psc-Su(z)2 (P3C) double mutant background (midline, straight dashed line; VNC border, curvy dashed line). Dpn and Hb channels of insets are shown individually at the right. **b,** *Left:* Abd-B expression in lateral view, mid-embryogenic embryos (dorsal, down). *Right:* ventral view of late-stage embryos. **c,** *Top:* total histone, H3, or PcG-associated mark, H3K27me3, immunostained with pan-neuroblast marker, Worniu (Wor) in stage 14 WT embryos. Gray scale image shows histone channel alone. Orange dashed line shows VNC border. Anterior is to the left in all panels.



Supplemental Figure 7 (related to Figure 6): Scatter plots for early competence window in *E(z)* and *Psc* and mutants.

a, *Left*: Average early competence window. *Right*: Scatter plots showing the number of Hb^{HA+} neurons relative to the number of Eve^{+} cells in each NB7-1 lineage analyzed. **b,** *Left*: Average early competence window. Two Psc null alleles (Psc^{h27} and Psc^{e24}) are shown. Scatter plots shown to the right. All data are represented as mean ± SD.